HHS Public Access

Author manuscript

Mater Today Adv. Author manuscript; available in PMC 2022 October 07.

Published in final edited form as:

Mater Today Adv. 2022 August ; 15: . doi:10.1016/j.mtadv.2022.100261.

Silk fibers assisted long-term 3D culture of human primary urinary stem cells via inhibition of senescence-associated genes: Potential use in the assessment of chronic mitochondrial toxicity

Huifen Ding[a,b], **Sunil George**[a], **Xiaoyan Iris Leng**[c], **Michael Ihnat**[d], **Jian-Xing Ma**[e], **Guochun Jiang**[f], **David Margolis**[f], **Julie Dumond**[g], **Yuanyuan Zhang**[a,*]

[a]Wake Forest Institute for Regenerative Medicine, Wake Forest University Health Sciences, Winston-Salem, NC, USA

[b]Stomatological Hospital of Chongqing Medical University, Chongqing Key Laboratory of Oral Diseases and Biomedical Sciences, Chongqing Municipal Key Laboratory of Oral Biomedical Engineering of Higher Education, Chongqing, China

[c]Division of Public Health Sciences, Department of Biostatistics and Data Science, Wake Forest School of Medicine, Winston-Salem, NC, USA

[d]Department of Pharmaceutical Sciences, University of Oklahoma College of Pharmacy, University of Oklahoma Health Sciences Center, Oklahoma City, OK, United States

[e]Department of Biochemistry, Wake Forest University Health Sciences, Winston-Salem, NC, USA

[f]University of North Carolina HIV Cure Center, UNC Chapel Hill, Chapel Hill, NC, USA

[g]Division of Pharmacotherapy and Experimental Therapeutics, UNC Eshelman School of Pharmacy, UNC Chapel Hill, Chapel Hill, NC, USA

Abstract

Despite being widely applied in drug development, existing *in vitro 2D cell-based* models are not suitable to assess chronic mitochondrial toxicity. A novel *in vitro* assay system mimicking in vivo microenvironment for this purpose is urgently needed. The goal of this study is to establish a 3D cell platform as a reliable, sensitive, cost-efficient, and high-throughput assay to predict

*Corresponding author. yzhang@wakehealth.edu (Y. Zhang).

Declaration of competing interest

The authors declare that they have no known competing financial interests or personal relationships that could have appeared to influence the work reported in this paper.

Credit author statement

Huifen Ding: Methodology, Validation, Investigation, Formal analysis, Software, Writing – original draft, Visualization.; Sunil George: Investigation, Writing – original draft.; Xiaoyan Iris Leng: Formal analysis, Writing- Reviewing and Editing.; Michael Ihnat: Writing- Reviewing and Editing.; Jian-Xing Ma: Writing- Reviewing and Editing.; Guochun Jiang: Writing- Reviewing and Editing; David Margolis: Writing- Reviewing and Editing; Julie Dumond: Writing- Reviewing and Editing; Yuanyuan Zhang: Conceptualization, Methodology, Validation, Writing – original draft preparation, Writing- Reviewing and Editing, Visualization, Funding acquisition.

Appendix A. Supplementary data

Supplementary data to this article can be found online at https://doi.org/10.1016/j.mtadv.2022.100261.

drug-induced mitochondrial toxicity. We evaluated a long-term culture of human primary urine-derived stem cells (USC) seeded in 3D silk fiber matrix (3D USC-SFM) and further tested chronic mitochondrial toxicity induced by Zalcitabine (ddC, a nucleoside reverse transcriptase inhibitor) as a test drug, compared to USC grown in spheroids. The numbers of USC remain steady in 3D spheroids for 4 weeks and 3D SFM for 6 weeks. However, the majority (95%) of USC survived in 3D SFM, while cell numbers significantly declined in 3D spheroids at 6 weeks. Highly porous SFM provides large-scale numbers of cells by increasing the yield of USC 125-fold/well, which enables the carrying of sufficient cells for multiple experiments with less labor and lower cost, compared to 3D spheroids. The levels of mtDNA content and mitochondrial superoxide dismutase$_2$ [SOD2] as an oxidative stress biomarker and cell senescence genes (RB and P16, p21) of USC were all stably retained in 3D USC-SFM, while those were significantly increased in spheroids. mtDNA content and mitochondrial mass in both 3D culture models significantly decreased six weeks after treatment of ddC (0.2, 2, and 10 μM), compared to 0.1% DMSO control. Levels of complexes I, II, and III significantly decreased in 3D SFM-USC treated with ddC, compared to only complex I level which declined in spheroids. A dose- and time-dependent chronic MtT displayed in the 3D USC-SFM model, but not in spheroids. Thus, a long-term 3D culture model of human primary USC provides a cost-effective and sensitive approach potential for the assessment of drug-induced chronic mitochondrial toxicity.

Keywords

Mitochondrial toxicity; Antiviral drugs; 3D cellular assay; Human stem cells; Silk fibers; Spheroids

1. Introduction

Considerable progress in drug therapy has been paralleled by increasing awareness of potential adverse drug outcomes. As a result of the universal presence of mitochondria and their critical roles in cellular metabolism [1], the adverse drug-mitochondrial interactions often exhibit clinical toxicity in multiple organs such as liver [2–4], kidneys [5–7], heart [8,9], brain [10], skeletal muscle [11,12] and fat [13] tissues. Understanding these adverse effects could help predict potential mitochondrial toxicity (MtT) of new drugs and adjust drug regimens to improve individual patient safety. Despite often being used in drug-induced toxicity testing, two-dimensional (2D) cultures cannot accurately mimic the 3D tissues in vivo with cell-cell and cell-extracellular matrix interactions [14]. Cells proliferate and their mitochondria replicate rapidly in 2D models, which is not appropriate for MtT assessment [1]. In addition, *in vitro* 2D cultures with immortalized cell lines resulted in 95% drug response failure rate in human subjects [15]. In vitro three-dimensional (3D) models of human primary cells promise to bridge the gap between traditional 2D cell culture and in vivo animal models, allowing a direct assessment of mitochondrial metabolism in human cells.

In most *in vitro* toxicity assessment, the timeline for determining the drug impact is from 24 h to one week. However, for individuals with human immunodeficiency virus (HIV) infection, antiretroviral therapy (ART) has been administered for their lifetime. Some

ART might cause delayed MtT. Thus, chronic MtT testing is critical to assess cumulative toxicities of anti-HIV drugs. The longer the 3D culture, the more MtT information can be gained. Based on our recent studies, most cells (90%) in 3D spheroids are viable after 4 weeks culture [1]. As a human cell culture *in vitro* will only divide 50 times, on average [16], the lifespan of human cells is limited. In addition, optimal times for cell culture for MtT testing depends on the culture conditions in which most cells remain alive and healthy. Thus, 6–10 week culture would be the favorable time for most human cells to predict the earliest stages of chronic MtT. However, using cells from healthy individuals for drug-toxicity testing might not replicate late toxicities after years of ART. Autologous cells from patients with HIV or individuals at high risk for HIV on pre-exposure prophylaxis (Pr-EP) therapy in a 3D culture could better reflect chronic MtT after years of ART.

Standard MtT testing requires reliable large-scale numbers of cells for serial assessments. As one of the 3D cell culture models, spheroids have been commonly used in new drug development to closely mimic the main structural and functional features of human solid tissues [17]. Human primary hepatocytes remain in 3D spheroids for long-term cultures (3–5 weeks) [18,19], however, 3D spheroid systems cannot provide sufficient largescale cells (such as half million cells/well). Because optimal sizes of spheroids require less than 350 μm with cell concentration ranging from 2000 to 8000 cells/spheroid to prevent necrosis at the center of 3D spheroids [20]. Creating large numbers of human primary cells in 3D spheroid cultures is time-consuming, labor-intensive, and expensive [21]. In addition, the maximal time frame for testing drugs are 4 weeks in most 3D spheroids with human primary cells [1]. Therefore, an improved cost-effective long-term 3D culture method with high cell numbers and good biological stability of primary human cells is needed for testing chronic ART-MtT.

Biomaterials with porous microstructures can hold large amounts of cells for long-term culture (>4 weeks) for tissue engineering and repair [22–31], which might provide a solution for *in vitro* 3D models for drug testing. These biomaterials include natural bio-matrixes, such as spider silk [32], chitosan [33], and microspheres made from collagen [34,35], gelatin [36,37], fibrinogen [38], hyaluronic acid [35], alginate [39]) and synthetic materials (PGA [37], PLGA [40], PLLA [41–43]). As a natural biopolymer. silk fibroin possesses outstanding characteristics with biocompatibility, biodegradability, durability, and flexibility [44] for regenerative medicine uses [45–49]. Fiber bio-matrixes with high porosity have interconnected pore networks, which provide anchoring sites to hold the cells together and facilitate nutrients, oxygen diffusion and waste removal for efficient cell growth during long-term 3D culture [50]. Thus, we anticipate that 3D porous silk fiber matrix (SFM) can provide an optimal long-term carrier for chronic MtT assessment.

Several types of drugs such as antiretroviral therapy (ART), anticancer drugs, antibiotics, and other classes of drugs can induce chronic MtT [51–53]. Zalcitabine (ddC), one of the first-generation nucleoside reverse transcriptase inhibitors (NRTIs) as a well-known ART agent, effectively inhabits HIV replication but induces severe MtT as patients need lifelong administration of ART. Although ddC has been removed from the market and listed by the U.S. Department of Health and Human Services (HHS) panel as a drug that should not be used due to its MtT [54], we use ddC as a test drug for a positive control to text chronic

MtT in this *in vitro* 3D cellular assay study, 0.1% DMSO (known for non-inducing MtT) as a control.

Human cell lines or animal primary cells are mostly used in existing *in vitro* cell assays. Although these cell lines are preferably used for convenience as they are easy to handle, they have an absence of human tissue-specific cytoarchitecture. Here, we demonstrate, for the first time, that stem cells exist in urine called urine-derived stem cells (USC) [55–57]. These cells, obtained via a non-invasive and low-cost approach, possess robust renewal capacity for tissue regeneration [22,24,55–87]. The rationale in using USC to assess MtT is that USC contain rich intracellular mitochondria and mitochondrial DNA remains stable in 3D culture system (in press). In addition, USC are easily accessible (urine) via non-invasive approaches [88], which is an optimal cell source to evaluate personalized mitochondrial toxicology. Furthermore, USC can be specifically used to test MtT in renal cells or for nephrotoxicity screening [20], since USC originate from the kidneys and efficiently differentiate into renal tubule epithelial and other renal cells, expressing renal proximal tubule cell (AQP1) and podocyte (synaptopodin and nephrin) biomarkers [20]. Thus, use of human primary cells, instead of cell lines or animal cells, is key to successfully establishing a reliable 3D culture system for new drug discovery and for monitoring patient- or disease-related cellular toxicology.

The goal of this study is to develop *in vitro* 3D long-term culture systems and determine the beneficial role of highly porous silk fiber matrix (SFM) on long-term human primary USC cultures used for assessment of ART-induced chronic mitochondrial dysfunction. Our data demonstrated that the silk fiber network provides a suitable microenvironment for 3D long-term culture with a sufficient amount of human primary USC without the induction of cell senescence and oxidative stress. Further, the anti-HIV drug ddC significantly decreased mitochondrial DNA (mtDNA) content, mitochondrial respiration, and ATP production in 3D long-term culture models, compared to 2D culture.

2. Material and methods

2.1. Materials

2.1.1. Silk fibroin and drugs—Silk fibroin was extracted from silk cocoons (TTSAM, China), according to the methods as previously reported [49]. Zalcitabine (ddC) is a well-known anti-HIV drug inducing MtT as a test drug in this study, which was provided from the NIH HIV reagent program (https://www.hivreagentprogram.org), dimethyl sulfoxide (DMSO) is a known negative control for MtT, was purchased from Sigma (St. Louis, Mo.).

2.2.2. Culture medium and supplements—Human USC were cultured in combined media: Keratinocyte serum-free medium (KSFM) and progenitor cell medium (1:1) as previously reported [55]. Briefly, KSFM was supplemented with 5 ng/ml epidermal growth factor, 50 ng/ml bovine pituitary extract, 30 ng/ml cholera toxin, 100 U/ml penicillin and 1 mg/ml streptomycin. Progenitor cell medium contained ¾ Dulbecco's modified Eagle's medium, ¼ Hamm's F12, 10% fetal bovine serum (FBS), 0.4 μg/ml hydrocortisone, 10^{-10} M cholera toxin, 5 ng/ml insulin, 1.8×10^{-4} M adenine, 5 μg/ml transferrin plus 2×10^{-9} M 3,39,5-triiodo-L-thyronine, 10 ng/ml epidermal growth factor (EGF), 10% penicillin and

streptomycin, were all purchased from Gibco (Thermo Fisher Scientific, Waltham, MA, USA). Acetone, ethanol, methanol, isopropanol, phosphate buffered saline (PBS) and all other reagents were used in this study. Demineralized water was used in all cases.

2.2. Methods

2.2.1. Preparation of silk fiber matrix—Silk fibroin (10%) electrospinning solution and random-structured matrix were collected using a wet process. Briefly, the sponge-like silk fiber matrixes (SFM) were assembled in a100% ethanol (Warner Graham Company, USA) bath up to 45 min. After fully cross-linked with ethanol and washed, the SFM samples were frozen with deionized water in a culture dish at dimeter 6 cm (Corning, NY). All SFM samples were lyophilized for 3 days.

Two sizes of SFM were made by Biopsy Dermal Punches (Painful Pleasures, USA) for different applications (Table 1 and Supplement Fig. 1): i) Small size SFM (s-SFM, 4 mm at diameter and 0.2 mm in thickness) fitted into a 96-well plate with ultralow attachment (ULA) U bottom (Corning, NY), which is used for measuring cell growth curves, live/dead assays and immunofluorescence for SOD2; ii) large size SFM (l-SFM, 8 mm at diamante and 1 mm) fitted to 12-well or 6-well ULA plate (Corning, NY) is used for the evaluation of mitochondrial function (complex I–V) by Western blot and mitochondrial DNA copy number by q-PCR that requires large numbers of cells.

2.2.2. Collection, isolation, and culture of human primary urinary stem cells —Human urine samples were collected from 12 healthy male donors aged from 17 to 65 years. Cell pellets were washed with PBS following urine samples being centrifuged. The cells were plated in culture plates with USC medium. USC were cultured at 37 °C in a humidified atmosphere of 5% CO_2. Cells at passage (p) 3 were used for all the groups and tests. To assess cell morphology, proliferation and live/dead, USC were seeded into 96-well plates in three culture conditions: i) 2D culture (4 × 10 [3] cells/well); ii) 3D sphere in 96-well plates with ULA (4 × 10 [3] cells/well); iii) 3D s-SFM in 96-well plates with ULA (4 × 10 [3] cells/s-SFM/well), respectively. To generate larger numbers of cells for Western-blot analysis, USC were cultured either in l-SFM for 3D USC-SFM in 12-well or 6-well ULA plates (5 × 10 [5] cells/l-SFM/well) or in Micro-molds (Microtissues 3D Petri Dish (Sigma, USA)) for 3D spheres with 88 wells. Culture media were changed every other day.

2.2.3. Live/dead assay—Cell viability of USC within spheroids and SFM was examined using a live/dead assay (Thermo Fisher) at week 1, 2, 4, 6 and 8. These time points are based on slow cell growth rates as the population doubling times are ranged from 1 to 4 weeks in 3D spheroids depending on cell types [1]. Calcein AM and EthD-1 were diluted by PBS into 2 mM and 4 mM working solutions, Cell construct samples were washed with PBS, and incubated in the working solution for 30 min in room temperature (RT). After washed with PBS following staining, USC within 3D culture samples were observed under confocal microscope (Leica TCS-LSI, Leica Biosystems Inc. Buffalo Grove, IL) or an Olympus IX-70 fluorescence microscope.

2.2.4. Cell proliferation assays—Cell proliferation or viability was measured at different time points after USC were seeded on 2D, spheroids and 3D-SFM in 96-well plates, respectively, assessed by Cell Counting Kit-8 (CCK-8 assay, Dojindo, Japan), according to manufacturer's instructions (Fig.1D). The absorbance at 450 nm was measured using microplate reader (MultiSkan FC, Thermo, USA).

To evaluate the maximum amount cell numbers capable of being cultured on 3D USC-SFM, different cell numbers (10 [6],10^5,10^4, and 4 × 10 [3] cells/well) in 220 μl culture medium were seeded on s-SFM in ULA 12-well plates for 6 weeks and assessed by CCK-8 as above (Fig. 2). To allow cells efficiently attach the SFM scaffolds, USC seeded on s-SFM were incubated for 2 h and then extra 200 μl culture medium was added. USC-SFM were transferred from 96-well to 12-well plate 12 h after initial seeding with enough medium the next day.

2.2.5. Ultrastructure of 3D cultures—A scanning electron microscope (SEM) was used to evaluate the surface morphology of spheroids and USC-SFM. Both types of 3D culture samples were fixed in 2.5% glutaraldehyde and dehydrated using a Leica EM CPD300 Critical Point Dryer (Leica Microsystems GmbH, Wetzlar, Germany), then mounted and sputter-coated with gold sputtering. The cell samples were examined under FlexSEM 1000 Scanning Electron Microscopy (Hitachi Medical Systems America Inc., Twinsburg, OH, USA) at an accelerating voltage of 10 kV and working distance of 6 mm.

2.2.6. USC treated with ddC at different doses at 2- and 6-week—To determine the dose effect of ddC on cell viability, mitochondrial function and oxidative stress of USC in both 3D cultures: spheroids and USC-SFM, we added ddC at different doses: 0.2, 2 and 10 μM^1 in the culture medium every 2 days, 3 replicates per concentration. To evaluate the time-dependent effect of ddC on USC in 3D cultures, spheroids and USC-SFM samples were assayed 2–6 weeks after administering ddC, 3 replicates per time point. DMSO (0.1%) was used as a control.

2.2.7. Immunohistochemical assessment of mitochondrial superoxide dismutase—To assess mitochondrial superoxide dismutase 2 (SOD2) levels, both spheroids and USC-SFM samples were fixed with 4% PFA for 30min, permeabilized by 0.2% Triton-X 100, and blocked by DAKO protein block. The cell samples were incubated in primary antibodies anti-human SOD2 (Cell Signaling Technology, USA, diluted 1:50, Danvers, MA) overnight at 4 °C. Secondary antibody (Goat anti-Mouse, Alexa Fluor⁻™ 647, Thermo Fisher Scientific, USA, diluted 1:200) was then applied for 2 h at RT. Cell nuclei were stained by DAPI and then observed by an Olympus FV10i® confocal laser scanning microscope.

2.2.8. Real time-PCR—To measure the levels of cell senescence genes (p13, 21 and Rb) [92] and mitochondrial DNA (mtDNA) content, we assessed mRNA expression of spheroid (n = 3) and 3D USC-SFM (n = 3) samples using BioRad CFX connect Real-time PCR Detection System [93]. Genomic DNA was extracted from the cells using a DNeasy Blood & Tissue Kit (Qiagen, Valencia, Cat. No 69504) according to the manufacturer's protocol. Q-PCR recipe was a mix with SYBR Green SuperMix (ThermoFisher, USA, Cat.

No 4367659) using both the mitochondrial and the nuclear primers [93] (Table 2) and the temperature cycling was used: initial denaturing at 50 °C for 2 min, 95 °C for 15 min, followed by 40 cycles of denaturing at 95 °C for 30 s, annealing at 60 °C for 1 s and extension at 95 °C for 15 s, 60 °C for 1 min, annealing at 95 °C for 15 s, 60 °C for 1 min and dissociating at 95 °C for 15 s.

To determine mRNA expression of ddC-treated USC in 3D cultures, the mRNA was extracted by RNeasy Mini Kit (Qiagen, Valencia, Cat. No 74104) and reversed to cDNA by High-Capacity cDNA Reverse Transcription Kit (Thermo Fisher, USA, Cat. No 4368814). The other reagents and the primers were the same as Real time-PCR for mtDNA (Table 2). The PCR temperature cycling used: initial denaturing at 50 °C for 2 min, 95 °C for 10 min. The rest of the process is the same as the Real time-PCR for mtDNA. The reference is normalized by the geometric mean of GAPDH, POLR2A and PGK1.

2.2.9. Western blot analysis for complexes I–V and SOD2—To generate sufficient cell numbers for immunoblot analysis, USC (5 × 10 [5] cells) within spheroids and l-SFM were loaded in 81-well molds made by Micro-Tissues 3D Petri Dish (Sigma, USA). USC in 2D culture were seeded into a 6-well plate at a density of 5 × 10 [5] cells/well as control. After a wash of the cell samples with PBS, the USC were harvested and incubated for 30 min in the presence of 500 μl of lysis buffer (Pierce, Rockford, IL) with 1% protease/phosphatase inhibitor cocktail (Cell Signaling Technology, Danvers, MA), vortexing every 5 min during incubating. The lysate was clarified by centrifugation, and protein concentrations were tested by Pierce™ BCA Protein Assay Kit. Following separation in 15% SDS-PAGE gels, the proteins were transferred onto a PVDF membrane (ThermoFisher) by a Bio-Rad Trans-Blot SD Semi-Dry Transfer Cell under 12 V for 1 h.

Individual activity of oxidative phosphorylation complexes I, II, II IV, V^{94} and mitochondrial SOD2 in USC before or after treatment with ddC at three doses were assessed. The membrane was blocked for 30 min in PBS–0.1% Tween 20 (PBST) containing 5% bovine serum albumin (BSA), washed with PBST, and incubated with the primary antibodies (Table 3) for 2 h or 4 °C overnight, diluted by PBST containing 5% BSA. After extensive washing with PBST, the membrane was incubated in the secondary antibodies correspondingly for 1 h at room temperature. The washed membrane was treated with an Immobilon ECL Ultra Western HRP Substrate (Millipore Sigma) and analyzed with a Fujifilm LAS-3000 Luminescent Image Analyzer system.

2.2.10. Statistical analysis—Descriptive statistics are presented as mean ± standard deviation (SD), GraphPad Prism software version 9.0. All data shown are derived from experiments that were independently repeated at least three times. For any experiment with multiple treatments, such as different doses, one-way ANOVA with Dunnett's multiple comparisons to control group (DMSO) or multiple unpaired t tests were used. For any experiment with two groups, such as different time points, student's t-test was used to make comparisons. Bonferroni's multiple comparisons were applied whenever appropriate. For all analyses, overall statistical significance was set at $\alpha = 0.05$.

3. Results

3.1. Fabrication of 3D silk fiber matrix

The diameter of silk fibers, porosity, and pore size of the SFM were optimized and characterized as we previously reported [49], leading to direct implications for cellular functionality and cell behavior *in vitro.* Both s-SFM and l-SFM were fabricated for different proposes (Table 1 and Supplement Fig. 1). The 3D SFMs at different sizes retained the entire porous structure without degradation in culture medium for more than 10 weeks. SFM was not affected by lysis buffer during protein or DNA/RNA extraction processes. In addition, SFM alone did not affect protein and gene expression assayed by Western blot and q-PCR.

3.2. Cell growth and viability of USC

In 2D culture, USC constantly proliferated and displayed over-confluence with the number of cells reaching the peak at weeks 4 and starting to decline at weeks 6 and 8 (Fig. 1 A&B). Cells formed “hills” with multiple layers on some areas (while arrows) and “valleys” with a single layer of cells on other areas for 6 weeks. This was due to aging USC that detached while the remaining USC with self-renewing properties started to proliferate and covered a“valley” region. Finally, some USC in 2D culture detached; some cells at large size still left on the culture dishes 8 weeks after initial plantation.

The sizes of spheroids were retained similar during 8-week culture, however cells at outer layers became larger in size; the bodies of spheroids appeared semi-transparent at 2 weeks but became darker at week 6 and 8, indicating that unhealthy cells existed in the center of spheroids with time. In addition, these solid cell spheroids lacked channels or spaces from the outer layers to the center of 3D spheroid.

In 3D SFM, USC attached, grew along silk fibers, and aggregated at the connecting points of silk fibers in 3D constructive matrix, more spaces among cells opened during 8-week culture to allow the culture medium flow passing through (Fig. 1A). To improve the potential of SFM to hold more living cells in long-term culture, we optimized the cell density of USC in different sizes of SFM. When cell growth curves and live/dead analysis were performed in 3D s-SFM, the number of USC was stable in s-SFM for 6 weeks, then declined at week 8; whereas the number of cells remained constant in 3D spheroids at week 4 but significantly decreased at week 6 ($p < 0.01$, Fig. 2). In addition, live/dead analysis showed an intense green fluorescence signal for live cells and a faint red fluorescence signal for death cells, indicating the majority cells remained viable in the 3D silk fiber network (Fig. 1B) after 2, 4, 6 and 8 weeks of incubation. Although the number of cells decreased in Fig. 1B, higher viability was observed in 3D SFM at week 8 in Fig. 1C. In contrast, 3D USC spheroids displayed an intense red fluorescence at the center at week 6 (Fig. 1C), indicating substantial cell death and matching the number of cells in spheroids decreasing at week 6 (Fig. 1B). Thus, the ultimate timing to test late mitochondrial function in 3D USC-SFM was found to be week 6 while the proper timing for testing drug induced MtT in 3D spheroids was at week 4.

3.3. Mitochondrial DNA content and ultrastructure of USC

Importantly, USC did not proliferate in 3D SFM and spheroids (Fig. 1B), and mitochondrial DNA (mtDNA) copy numbers were similar in 3D USC-SFM between 2 and 6 weeks after culture (Fig. 2A), which is preferred for mitochondrial function testing because the copy number of mitochondrial retained stable without replicating. In contrast, levels of mtDNA content significantly increased from Week 2–4. In addition, mitochondrial biogenesis is the cellular process that produces new mitochondria, which effectively causes an increase in mitochondrial mass [94]. Thus, mitochondrial biogenesis of 3D USC-SFM remained stable as compared to spheroids in 6-week culture (Fig. 2 B). These data indicate that mitochondrial DNA copy number retains more consistency in 3D USC-FSM than that in spheroids, which makes USC-FSM more suitable for MtT testing.

Ultrastructurally, the apical membrane facing the tubular lumen of normal renal proximal tubule epithelial cells (RPTEC) is folded and covered by brush border (microvilli) that increases transport area as an absorptive function characteristic [95]. Microvilli appeared on the surface of USC in 3D SFM and spheroids during 4-week culture (Fig. 3), indicating that 3D cultures of USC possess certain reabsorption properties of RPTEC.

3.4. Ample numbers of USC aggregated within SFM

To determine the maximal cell numbers of USC loaded in 3D SFM, we used different cell numbers (10 [6], 10^5, 10^4, and 4 × 10 [3] cells/s-SFM sample/well) in 220 μl culture medium in 12-well ULA plates for 8 weeks, assessed by CCK-8 (Fig. 4). When USC at 10^6 cells/well are loaded into s-SFM, only 1/2 of USC (i.e., 5 × 10 [5] cells) were retained 24 h after seeding and the half of cells were washed away following medium changes, indicating that the maximal number of cells carried in s-SFM are 5 × 10 [5] cells/s-FSM (Ø at 4 × 0.2 mm^3). The number of USC in s-SFM at 4 × 10 [3],1 × 10 [4] 1 × 10 [5] and 5 × 10 [5] cells/well were stably retained without significant cell proliferation during 6-week culture, but significantly decreased at week 8 ($p < 0.05$).

Although s-SFM can carry a maximum number of cells at 5 × 10 [5] cells with high cell viability for 8 weeks, the medium must be changed two times a day to maintain cell viability when cultured in 96-well plates. To perform a better comparison of the cell growth curve and viability, we seeded the same cell density at 4 × 10 [3] USC in 2D culture, spheroids and 3D SFM, respectively. The CCK-8 test provided a reliable assay to test cell viability for 2D cultures or for small size 3D cultures or spheroids.

In addition, USC aggregated and attached at the silk fiber and the network connecting points to form 3D cell constructs with a large scale of cells (5 × 10 [5] cells/well) in l-SFM, which is about 125-fold higher than USC grown as 3D spheroids in 96-well plates (4 × 10 [3]cell/well). Serial MtT assessments often require up to 5 × 10 [6]cells/sample [96], 3D l-SFM in a 12-well plate provides enough cells (6 × 10 [6]/plate) to meet these large cell requirements.

3.5. Mitochondrial SOD2 expression in USC

Western blot analysis showed that protein levels of mitochondrial SOD2 (mt-SOD2) in 3D USC-SFM and 2D culture remained low 2 and 6 weeks after culture, while protein levels of SOD2 significantly increased in 3D USC spheroids (Fig. 5 A&B). Dual immunofluorescence staining also demonstrated that the expression levels of SOD2 in 3D USC-SFM and 2D culture were significantly lower than those in spheroids (Fig. 5C&D). Because of a mitochondrial antioxidant role of SOD2, the increased expression of SOD2 indicates that USC in spheroids were under more oxidative stress, than in 2D culture or 3D USC-SFM.

3.6. Senescence gene expression in USC

The expression of senescence-related genes (p13, 21 and Rb) [92] of USC in 3D USC-SFM was significantly lower than those in 3D spheroids ($p < 0.05$) (Fig. 6). This indicates that silk-fiber networks provide the appropriate microenvironment for USC growth by preventing the expression of senescence-related genes in 3D structures during long-term culture. In addition, lower expression of senescence-related genes was found in 2D culture. This might be due to the occurrence that only USC with self-renewal potential remain on the 2D cell dish and continue to overgrow or that aging cells were detached and washed away during 6-week culture. In addition, cells in the 2D culture have easily access to the medium for metabolites and nutrient exchange, potentially leading to increased proliferation.

3.7. ddC-induced chronic cytotoxicity assessment

The antiretroviral drug ddC significantly affected cell viability and growth of USC in 2D culture. Cells readily detached with few cells remaining on the dishes 2 weeks after ddC treatment. In contrast, ddC did not significantly affect cell survival and growth 3 days, 1, 2, 4, and 6 weeks after culture in 3D USC-SFM (Fig. 7A).

3.8. Levels of oxidative phosphorylation complexes I–V decreased after ddC treatment

MtT assessments showed that ddC induced significant impairment of mitochondrial function by inhibiting oxidative phosphorylation complex I-IV in 3D culture models, which featured as: **i**) in Fig. 7B&C, the levels of complex I, and IV significant decreased 2 weeks after being treated with ddC at middle and high doses (2 and 20 μM), compared to ddC at the low dose (0.2 μM); the levels of complex I, II, III and IV significantly declined 6 weeks after treated with middle and high dose ddC (2 and 20 μM), compared to those in ddC at low dose (0.2 μM). This data indicates that the dose-dependent MtT of ddC can be detected in 3D USC-SFM during 6 weeks culture; **ii**) complex I-IV levels in 3D USC-SFM significantly decreased in response to ddC at 2 and 20 μM at 6 weeks compared to 2 weeks, indicating that a time-dependent MtT of ddC developed in 3D USC-SFM model in Fig. 7 B&C; **iii**) in Fig. 7B&E, the levels of complexes II, III and IV in 3D USC-SFM significantly decreased by ddC at (2 and 20 μM), compared to complex levels in spheroids. In addition, levels of complexes I, II and IV significantly increased after being treated with low dose ddC (0.2 μM) in 3D spheroids, which did not occur in 3D USC-SFM. The data indicated that the 3D USC-SFM model was more sensitive and reliable to detect drug-induced MtT, as compared to 3D spheroids. Thus, the data indicated that ddC induced mild cytotoxicity but

a significant dose- and time-dependent mitochondrial toxicity as represented by decreasing levels of complexes I-IV in USC in both spheroids and 3D SFM, but that 3D USC-SFM is more sensitive in detecting oxidative phosphorylation complex proteins than 3D spheroids.

3.8. Expression of mtDNA declined after ddC treatment

To determine the adverse effect of ddC on mtDNA in 3D cultures, we quantified the copy numbers of mtDNA by competitive PCR in the specimens of 3D cultures after treatment with ddC. ddC significantly decreased the levels of mitochondrial DNA content (Fig. 8A) and mitochondrial mass (Fig. 8B) in 3D USC-SFM ($p < 0.01$) in a time-dependent manner. However, this time-dependent effect was not displayed in 3D spheroids, which might be related to the low cell survival rate of USC in spheroids 6 weeks post treatment. In addition, ddC at 2 and 20 μM inhibited mtDNA content compared to those in both 3D cultures treated with 0.2 μM ddC at 2- and 6-weeks post treatment. There was no significant difference in mtDNA content in cultures treated with ddC between at 2 and 20 μM. Thus, like complex I-IV levels, ddC induced a time- and dose-dependent decrease in mitochondrial DNA copy number in USC in both 3D culture models while 3D USC-SFM model was more sensitive and reliable to detect drug-induced MtT than 3D spheroids.

4. Discussion

Mitochondrial dysfunction has been increasingly been identified as a potential etiology of drug-induced toxicity, in particular for chronic MtT in the individuals with HIV taking long-term or life-long ART. Based on our recently established *in vitro* 3D spheroid model for MtT [1] and nephrotoxicity assays [20], we explored a novel technology to provide 3D long-term (6-week) culture systems of human USC-SFM for chronic MtT assessment. Our data demonstrated that 3D *in vitro* models offered an increased microenvironmental control that can yield more predictive drug responses than 2D models. 3D SFM with porous structure supported large numbers of human primary stem cells in long-term culture, which provides a cost-effective approach suitable for assessing chronic ART-MtT. Innovative features of the 3D USC-SFM culture system for the assessment of chronic ART-MtT and novel traits of USC using in toxicity test are summarized in Table 4.

In vitro cell-based assays are often positioned within the drug-development process outline toxic screens to prevent adverse effects of new ART drugs. Traditional 2D cell cultures have made important contributions to drug discovery to offer the initial selection for drug compound screening. However, their limitations have been increasingly recognized, especially in MtT testing. Despite being most used in acute metabolic assays (<2 weeks), existing *in vitro* 2D assays of human cell lines or animal primary cells are not capable of detecting chronic MtT [45–48]. This is because most 2D cultured cells cannot survive or are detached from culture dishes for more than 2 weeks after administration of ART, although some cell lines, such as the HepaRG cell line, are capable of surviving in no toxic environment for 4 weeks [97]. In addition, cell lines that are commonly used in 2D cultures divide indefinitely, and sometimes express unique gene expression patterns not found in any cell type in the human body. These 2D monolayer cultures do not mimic 3D tissue or organ architecture having multiple cell types and tissue specific extracellular matrix (ECM).

Furthermore, cell lines proliferate rapidly in 2D conditions, such that mitochondrial numbers in cells increase with time, making it difficult to accurately measure the adverse effects of ART on mitochondrial DNA (mtDNA) content and mitochondrial function. Finally, drug availability to cells varies between *in vitro* 2D and body tissues. Drug molecules are readily accessible to each cell in 2D culture with a high ratio of drug molecule-to-cell number, leading to an underestimation of drug toxicity in clinical settings [98].

Increasing evidence has demonstrated that 3D cell culture systems are in many ways superior to those in 2D culture and are set to dominate *in vitro* studies in tissue regeneration, disease modeling, new drug discovery and toxicology testing [1,14,20]. Several types of 3D cultures have been used in drug testing: organoids, spheroids, 3D gel with cells, 3D culture of cell-matrix and chips [99]. The optimal assays for chronic MtT need to meet several criteria: **i**) long-term 3D culture assays (≥6 weeks), installed with porous microstructures supporting cell retention and enhancing gas, nutrition, molecular and drug distribution, and suitable for chronic MtT analysis; **ii**) selecting human primary cells, rather than cell lines or animal cells, that can be easily accessed and are desirable for engineering human tissue equivalents *in vitro*; **iii**) using stem cells that possess vigorous expansion capacity with rich mitochondria and mitochondrial DNA (mtDNA) [93] and are highly sensitive for the recognition of effects on mtDNA and mitochondrial function; **iv**) possess stable numbers of cells and mitochondrial copy numbers over time, which is suitable for determining the effect of ART on mtDNA content [1]; **v**) generating large-scale numbers of cells (i.e., 5 × 10 [6] cells/sample [96]) in 3D cultures that can be used for a series of MtT assessments, including reactive oxygen species (ROS), mitochondrial permeability transition, mitochondrial respiration, mitochondrial DNA content, apoptosis, and inhibition of beta-oxidation of fatty acids [51] using several assays, such as ELISA, immunofluorescence staining, colorimetric assays and Western blot analysis. Thus, the data generated from such a substantial number of cells from a single sample for multiple assays would be more accurate, sensitive and have little inter-laboratory variability, particularly for long-term exposures; and **vi**) providing a cost-effective platform with less labor and less time consumption by offering feasible cell-scaffold constructs for in vivo studies.

Despite being adopted in the drug discovery field, 3D spheroids with small number of cells limit their application for metabolic experiments [1,20]. Spheroids display an imperfection of an inherent gradient of molecules (i.e., O_2, nutrients, metabolites, or drugs), leading to a central necrotic core zone enclosed by quiescent cells and an outer layer of actively proliferating cells [52]. The maximum size of spheroids is limited between 300 and 400 μm and a small number of cells (4–8 × 10 [3] cells/sample/well) because of the diffusion limitation of ranging between 150 and 200 μm to O_2[53]. In addition, drug molecules cannot evenly distribute into the large size spheroids (>400 μm) due to the lack of channels or openings. *In vivo* solid tissues are provided with rich vessel systems, allowing even distribution of the drug molecules. However, it is a challenge for some drugs with high molecular weights to equally penetrate in 3D spheroids.

We proposed that 3D SFM with porous microstructures provide large-scale generation of human primary stem cells (5 × 10 [5] cells/well) (Table 1) with stable mitochondrial

qualities for long-term culture. Our previous studies demonstrated that despite no vasculature installed in vitro, porous biomaterial matrices significantly promoted vasculature and engraftment formation 4 weeks after in vivo implantation [22–31], compared to non-porous collagen-based matrix, indicating that a matrix with porous structure allowing vascular formation is critical to carry more cells for long-term culture. Thus, *in vitro* 3D models with porous constructs appear to mimic in vivo tissues with vessel channels, enhancing drug molecules to uniformly distribute into *in vitro* 3D cellular structures. The present study is the first to test this idea using a silk fiber network to support human primary cells to form 3D constructs (Fig. 1A) to assess drug-induced chronic MtT, although silk fibers have been used previously to produce scaffolds for tissue regeneration.

We demonstrated that 3D SFM with abundant porous microstructures favors cell survival and retains USC growth for 6-week culture. Silk fibers formed in a bundle with integrated human USC are both compacted and flexible, with favorable mechanical properties. In addition, the interconnected SFM porous matrix networks are essential to enable the transport of nutrients and drug molecules, removal of waste, and facilitate migration of cells, which are like the in vivo condition. The expression of senescence-related genes [44] of USC in 3D SFM is significantly lower than that in 3D spheroids. This indicates that silk-fiber networks provide the appropriate microenvironment for 3D long-term USC culture by down regulating of senescence-related gene expression. Although lower levels of senescence-related gene expression were found in 2D culture, this might be due to the fact that some USC with self-renewal potential remained on the dish and continued to grow after the over-matured cells were detached and washed away for up to 6 weeks.

Human primary USC as an optimal universal cell source were selected to use in this 3D model system because of their biological advantages for MtT assessment, including: **i**) As stem cells, USC are superior to existing other human somatic cell types in drug testing because of their regeneration capacity, providing cells in large numbers (>1 × 10 [8] USC at p3 three weeks after collection of 24-h' urine sample [85]); **ii**) these cells do not require tissue dissociation steps with digestive enzymes, thus better preserving cell viability; **iii**) USC contain abundant mitochondria in renal progenitor cells [1], and mitochondrial DNA remains stable with no replication in 3D culture system for 6 weeks, allowing us to assess ART-MtT; **iv**) autologous USC more accurately represent individual patient- or disease-related characteristics [65], which is different from immortalized cell lines and animal cells; **v**) USC, are easily accessible via a non-invasive approach, which offers clear advantages over stem cells from other sources; and **vi**). USC can be specifically used in testing MtT in the renal cells, or nephrotoxicity screening [20], since USC originate from the kidneys and efficiently differentiate into renal tubule epithelial and other renal cells, expressing a renal proximal tubule cell (AQP1) and podocyte biomarkers (synaptopodin and nephrin) [20].

Several drug classes (such as antiviral drugs, chemotherapeutic agents, antibiotics, and anti-tuberculosis drugs, drugs of abuse, and toxicants (i.e., radiocontrast agents, chemicals, industrial, or environmental toxic agents) [100] are recognized to induce MtT. Among antiretroviral agents, nucleoside reverse transcriptase inhibitors [NRTIs] and integrase strand transfer inhibitors [INSTIs] are most commonly used for fighting HIV/AIDS, HBV or co-

infection of HIV/HBV. Although HIV infection has no cure, ART can control viral growth and keep the patient healthy, extending life. However, long-term use of these ART drugs could increase morbidity and mortality among those with the viral infection. In addition, these drugs make up the majority of delayed clinical phase and post-market withdrawals, which causes the loss of immense revenue. Thus, it is critical to identify chronic MtT for the optimization of ART regimens. Drug-induced chronic MtT (≥4 weeks) affects people living with HIV over time during long-term ART. Multiple studies indicate that either HIV infection [4] or antiretroviral drugs [100] causes mitochondrial dysfunction, leading to cellular exhaustion, senescence, and apoptosis [101]. This highlights the urgent need for further investigation into AVT-induced mitochondrial compromise. As a classic NRTI, ddC was selected as a test drug in this study because it is a well-known anti-HIV agent causing MtT. ddC specifically inhibits mitochondrial toxicity in several cell types such as *T-lymphoblastoid cells* [102,103], *HeLa epithelial cells* [10], *HepG2* [52,53,104] *and HepaRG* [52,105], peripheral neuronal cells [106], skeletal myocytes, and renal proximal tubular epithelial cells. As USC are renal cells and stem cells with rich mitochondria, they are ideal cell sources to test the cellular toxicity of ddC in human primary cells.

An *In vitro* assay panel was performed to detect mitotoxicity [107] in 3D cultures of USC in this study, including cytotoxicity, oxidative phosphorylation complexes I–V, mtDNA copy number, mitochondrial mass, mitochondrial SOD2. ddC at 7–90 μM usually causes severe cytotoxicity of HepG2 cells and human primary skeletal muscle cells in 2D culture with 50% cell death [108]. We demonstrated that ddC induced mild cytotoxicity with cell death ratio at 5–10% in 3D USC-SFM at week 6, which is significantly different from 2D culture. Compared to 2D culture, cells often have more resistance to drugs in 3D culture as do in vivo conditions and provide more accurate data regarding cell–cell and cell-matrix interactions, drug distribution, and metabolic profiling. Porous scaffolds such as SFM with cells provides advantages of better drug metabolism and more accurate evaluation of drug effects [109].

Mitochondrial bioenergetic analysis (i.e., mitochondrial stress tests) can be performed using Seahorse technology that simultaneously analyzes the two main metabolic energy pathways: mitochondrial respiration and glycolysis or Western blot [110]. The assays provide insight into the cause of mitochondrial dysfunction and a more in-depth understanding of metabolic pathways, signals, and phenotypes in the cells. However, Seahorse technology often requires monolayer cells on 2D cultures, thus we used Western-blot to measure oxidative phosphorylation complexes I–V protein levels in this study. Despite mild cytotoxicity, ddC induced significant chronic MtT with the inhibition of complex I–V in a time- and dose-dependent manner, which is more sensitive than 3D spheroids. Thus, due to the capacity of mass production of primary human cells in long-term 3D culture with favorable cell viability, the 3D USC-SFM method is promising for the assessment of chronic ART-MtT. Similarly, a prolonged time-course reveals that ddC induced MtT via inhabiting mtDNA copy number and mitochondrial mass. Recent studies showed that Seahorse technology has been used in 3D spheroids to measure cellular respiration and to evaluate lactate release [111] although this technology has not been wildly used in 3D culture systems due to the technological limitations, particularly in the size of spheroids.

The levels of oxidative stress in 3D USC-SFM and 2D culture were significantly lower than those in 3D spheroids of USC. As a group of enzymes, SOD catalyzes the dismutation of superoxide radicals (O_2^{-*}) to molecular oxygen (O_2) and hydrogen peroxide (H_2O_2), providing a cellular defense against reactive oxygen species. SOD1 is in the cytoplasm, SOD2 is in the mitochondria while SOD3 is extracellular. SOD1 and SOD2 contain copper and zinc, whereas SOD2, the mitochondrial enzyme, has manganese in its reactive center. Increased mitochondrial SOD2 activity might decrease cell oxidant levels observed in 3D spheroids, suggesting a reaction to greater oxidative stress in the spheroid cultures than that in 3D USC-SFM and 2D culture.

Aside from key MtT assays used in this study, other assessments have been often used in the evaluation of mitochondrial dysfunction, including glycolytic flux for cell metabolic status and drug MtT, ATP production for energy metabolism disruption, reactive oxygen and nitrogen production and total glutathione expression for amplified free radical production, and caspase 3 activation for altered apoptosis [1]. Following establishing this long-term 3D culture assays, we will further test more ART and other drugs at different doses with a wide scope of mitochondrial function assays. A panel of drug lists at both positive and negative control is provided for MtT assessment in Table 5.

In summary, the present study demonstrated that the long-term in vitro 3D culture systems of human primary USC can predict MtT that 2D culture cannot achieve. *In vitro* 3D culture systems are superior to 2D culture in long-term culture and more accurate in testing chronic mitochondrial toxicity with neither cell proliferation nor mitochondrial replication occurring in the 3D USC cultures. 3D spheroid assays can be used in the measurement of the parameters requiring immune-fluorescence staining, and the evaluation of cellular respiration and lactate release with Seahorse technology. In addition, 3D USC-SFM can carry an ample number of cells for 6 weeks, are more sensitive and reliable in testing MtT, and are more physiologically relevant than 3D spheroids. Thus, 3D USC culture systems provide cost-effective and sensitive assays with less labor and reduced cost to test toxicant or drug induced chronic MtT via a series of experiments, compared to traditional 2D cultures.

5. Conclusions

We have developed novel *in vitro* 3D models with unique cell sources and natural silk fiber biomaterials which yield large scale production of long-term cultured human primary USC for a series of mitochondrial function analysis. In vitro 3D long-term culture platforms of USC potentially provide new opportunities in testing chronic MtT for new drug development and personalized toxicology. In vitro long-term 3D cultures developed in this study yield reproducible dose- and time-dependent chronic MtT, which is not possible in existing 2D cultures. Particularly, these *in vitro* 3D USC assays can also be used for testing nephrotoxicity as USC are renal progenitor cells. Because of the complexity of the in vivo system where multiple tissues are affected by drug toxicity, in ongoing studies, we are modifying 3D models by loading multiple cell types and ECM supporting specific tissue function to test various drugs. In the future, such 3D culture assays designed with USC from the patients with HIV or healthy individuals with pre-exposure prophylaxis could help determine whether chronic MtT is induced after long-term of ART. In addition, HIV

itself could contribute to mitochondrial dysfunction. HIV infection-induced mitochondrial dysfunction and premature T cell aging will also be studied. Thus, we can better understand and assess the ART-mediated MtT in the setting of HIV infection for the individual taking ART for life-long treatment. Not only can 3D assays of human primary stem cells limit the number of unsafe drugs, but they also promise to allow a whole generation of new drugs to prosper. It will facilitate establishing a personalized in vitro system to predict individual susceptibility and assess chronic MtT of new drugs, particular for life-long anti-HIV drugs.

Supplementary Material

Refer to Web version on PubMed Central for supplementary material.

Acknowledgment

We thank Ms. Lilly M. Wong for her editing. This project has been funded with Federal funds from the National Institute of Allergy and Infectious Diseases, National Institutes of Health, under Contract No. R21 AI152832 and R03 AI165170. (PI: Y. Z).

References

[1]. Ding H, Jambunathan K, Jiang G, Margolis DM, Leng I, Ihnat M, Ma J-X, Mirsalis J, Zhang Y, 3D spheroids of human primary urine-derived stem cells in the assessment of drug-induced mitochondrial toxicity, Pharmaceutics 14 (2022) 1042. [PubMed: 35631624]

[2]. Brinkman K, ter Hofstede HJ, Burger DM, Smeitink JA, Koopmans PP, Adverse effects of reverse transcriptase inhibitors: mitochondrial toxicity as common pathway, Aids 12 (1998) 1735–1744. [PubMed: 9792373]

[3]. Moyle G, Clinical manifestations and management of antiretroviral nucleoside analog-related mitochondrial toxicity, Clin. Therapeut. 22 (2000) 911–936, discussion 898.

[4]. Maagaard A, Kvale D, Mitochondrial toxicity in HIV-infected patients both off and on antiretroviral treatment: a continuum or distinct underlying mechanisms? J. Antimicrob. Chemother. 64 (2009) 901–909. [PubMed: 19740910]

[5]. Cote HC, Magil AB, Harris M, Scarth BJ, Gadawski I, Wang N, Yu E, Yip B, Zalunardo N, Werb R, Hogg R, Harrigan PR, Montaner JS, Exploring mitochondrial nephrotoxicity as a potential mechanism of kidney dysfunction among HIV-infected patients on highly active antiretroviral therapy, Antivir. Ther. 11 (2006) 79–86. [PubMed: 16518963]

[6]. Saumoy M, Vidal F, Peraire J, Sauleda S, Vea AM, Vilades C, Ribera E, Richart C, Proximal tubular kidney damage and tenofovir: a role for mitochondrial toxicity? AIDS 18 (2004) 1741–1742. [PubMed: 15280790]

[7]. Samuels R, Bayerri CR, Sayer JA, Price DA, Payne BAI, Tenofovir disoproxil fumarate-associated renal tubular dysfunction: noninvasive assessment of mitochondrial injury, AIDS 31 (2017) 1297–1301. [PubMed: 28323756]

[8]. Patel K, Van Dyke RB, Mittleman MA, Colan SD, Oleske JM, Seage GR 3rd, International Maternal Pediatric Adolescent ACTCST: the impact of HAART on cardiomyopathy among children and adolescents perinatally infected with HIV-1, AIDS (London, England) 26 (2012) 2027–2037.

[9]. Rana P, Aleo MD, Gosink M, Will Y, Evaluation of in vitro mitochondrial toxicity assays and physicochemical properties for prediction of organ toxicity using 228 pharmaceutical drugs, Chem. Res. Toxicol. 32 (2019) 156–167. [PubMed: 30525499]

[10]. George JW, Mattingly JE, Roland NJ, Small CM, Lamberty BG, Fox HS, Stauch KL, Physiologically relevant concentrations of dolutegravir, emtricitabine, and efavirenz induce distinct metabolic alterations in HeLa epithelial and BV2 microglial cells, Front. Immunol. 12 (2021) 639378. [PubMed: 34093527]

[11]. Arnaudo E, Dalakas M, Shanske S, Moraes CT, DiMauro S, Schon EA, Depletion of muscle mitochondrial DNA in AIDS patients with zidovudine-induced myopathy, Lancet 337 (1991) 508–510. [PubMed: 1671889]

[12]. Dalakas MC, Illa I, Pezeshkpour GH, Laukaitis JP, Cohen B, Griffin JL, Mitochondrial myopathy caused by long-term zidovudine therapy, N. Engl. J. Med. 322 (1990) 1098–1105. [PubMed: 2320079]

[13]. Gorwood J, Bourgeois C, Pourcher V, Pourcher G, Charlotte F, Mantecon M, Rose C, Morichon R, Atlan M, Le Grand R, Desjardins D, Katlama C, Fève B, Lambotte O, Capeau J, Bèrèziat V, Lagathu C, The integrase inhibitors dolutegravir and raltegravir exert proadipogenic and profibrotic effects and induce insulin resistance in human/simian adipose tissue and human adipocytes, Clin. Infect. Dis. 71 (2020) e549–e560. [PubMed: 32166319]

[14]. Edmondson R, Broglie JJ, Adcock AF, Yang L, Three-dimensional cell culture systems and their applications in drug discovery and cell-based biosensors, Assay Drug Dev. Technol. 12 (2014) 207–218. [PubMed: 24831787]

[15]. Hutchinson L, Kirk R, High drug attrition rates–where are we going wrong? Nat. Rev. Clin. Oncol. (2011) 189–190. [PubMed: 21448176]

[16]. Hayflick L, The limited IN vitro lifetime OF human diploid cell strains, Exp. Cell Res. 37 (1965) 614–636. [PubMed: 14315085]

[17]. Nunes AS, Barros AS, Costa EC, Moreira AF, Correia IJ, 3D tumor spheroids as in vitro models to mimic in vivo human solid tumors resistance to therapeutic drugs, Biotechnol. Bioeng. 116 (2019) 206–226. [PubMed: 30367820]

[18]. Bell CC, Hendriks DFG, Moro SML, Ellis E, Walsh J, Renblom A, Fredriksson Puigvert L, Dankers ACA, Jacobs F, Snoeys J, Sison-Young RL, Jenkins RE, Nordling Å, Mkrtchian S, Park BK, Kitteringham NR, Goldring CEP, Lauschke VM, Ingelman-Sundberg M, Characterization of primary human hepatocyte spheroids as a model system for drug-induced liver injury, liver function and disease, Sci. Rep. 6 (2016) 25187. [PubMed: 27143246]

[19]. Klaas M, Möll K, Mäemets-Allas K, Loog M, Järvekülg M, Jaks V, Long-term maintenance of functional primary human hepatocytes in 3D gelatin matrices produced by solution blow spinning, Sci. Rep. 11 (2021) 20165. [PubMed: 34635750]

[20]. Guo H, Deng N, Dou L, Ding H, Criswell T, Atala A, Furdui CM, Zhang Y, 3-D human renal tubular organoids generated from urine-derived stem cells for nephrotoxicity screening, ACS Biomater. Sci. Eng. 6 (2020) 6701–6709. [PubMed: 33320634]

[21]. Lee D, Pathak S, Jeong J-H, Design and manufacture of 3D cell culture plate for mass production of cell-spheroids, Sci. Rep. 9 (2019) 13976. [PubMed: 31562370]

[22]. Bodin A, Bharadwaj S, Wu S, Gatenholm P, Atala A, Zhang Y, Tissue-engineered conduit using urine-derived stem cells seeded bacterial cellulose polymer in urinary reconstruction and diversion, Biomaterials 31 (2010) 8889–8901. [PubMed: 20800278]

[23]. Tian H, Bharadwaj S, Liu Y, Ma PX, Atala A, Zhang Y, Differentiation of human bone marrow mesenchymal stem cells into bladder cells: potential for urological tissue engineering, Tissue Eng. 16 (2010) 1769–1779.

[24]. Wu S, Liu Y, Bharadwaj S, Atala A, Zhang Y, Human urine-derived stem cells seeded in a modified 3D porous small intestinal submucosa scaffold for urethral tissue engineering, Biomaterials 32 (2011) 1317–1326. [PubMed: 21055807]

[25]. Liu Y, Ma W, Liu B, Wang Y, Chu J, Xiong G, Shen L, Long C, Lin T, He D, Butnaru D, Alexey L, Zhang Y, Zhang D, Wei G, Urethral reconstruction with autologous urine-derived stem cells seeded in three-dimensional porous small intestinal submucosa in a rabbit model, Stem Cell Res. Ther 8 (2017) 63. [PubMed: 28279224]

[26]. Wei J, Han J, Zhao Y, Cui Y, Wang B, Xiao Z, Chen B, Dai J, The importance of three-dimensional scaffold structure on stemness maintenance of mouse embryonic stem cells, Biomaterials 35 (2014) 7724–7733. [PubMed: 24930853]

[27]. Tian H, Bharadwaj S, Liu Y, Ma H, Ma PX, Atala A, Zhang Y, Myogenic differentiation of human bone marrow mesenchymal stem cells on a 3D nano fibrous scaffold for bladder tissue engineering, Biomaterials 31 (2010) 870–877. [PubMed: 19853294]

[28]. Liu Y, Bharadwaj S, Lee SJ, Atala A, Zhang Y, Optimization of a natural collagen scaffold to aid cell-matrix penetration for urologic tissue engineering, Biomaterials 30 (2009) 3865–3873. [PubMed: 19427687]

[29]. Tian H, Bharadwaj S, Liu Y, Ma H, Ma PX, Atala A, Zhang Y, Myogenic differentiation of human bone marrow mesenchymal stem cells on a 3D nano fibrous scaffold for bladder tissue engineering, Biomaterials 31 (2010) 870–877. [PubMed: 19853294]

[30]. Wan Q, Xiong G, Liu G, Shupe TD, Wei G, Zhang D, Liang D, Lu X, Atala A, Zhang Y, Urothelium with barrier function differentiated from human urine-derived stem cells for potential use in urinary tract reconstruction, Stem Cell Res. Ther 9 (2018) 304. [PubMed: 30409188]

[31]. Lang R, Stern MM, Smith L, Liu Y, Bharadwaj S, Liu G, Baptista PM, Bergman CR, Soker S, Yoo JJ, Atala A, Zhang Y, Three-dimensional culture of hepatocytes on porcine liver tissue-derived extracellular matrix, Biomaterials 32 (2011) 7042–7052. [PubMed: 21723601]

[32]. Kumari S, Bargel H, Scheibel T, Recombinant spider silk-silica hybrid scaffolds with drug-releasing properties for tissue engineering applications, Macromol. Rapid Commun. 41 (2020), e1900426. [PubMed: 31697434]

[33]. Dhiman HK, Ray AR, Panda AK, Three-dimensional chitosan scaffold-based MCF-7 cell culture for the determination of the cytotoxicity of tamoxifen, Biomaterials 26 (2005) 979–986. [PubMed: 15369686]

[34]. Carey SP, Martin KE, Reinhart-King CA, Three-dimensional collagen matrix induces a mechanosensitive invasive epithelial phenotype, Sci. Rep. 7 (2017) 42088. [PubMed: 28186196]

[35]. Lou J, Stowers R, Nam S, Xia Y, Chaudhuri O, Stress relaxing hyaluronic acid-collagen hydrogels promote cell spreading, fiber remodeling, and focal adhesion formation in 3D cell culture, Biomaterials 154 (2018) 213–222. [PubMed: 29132046]

[36]. Afewerki S, Sheikhi A, Kannan S, Ahadian S, Khademhosseini A, Gelatin-polysaccharide composite scaffolds for 3D cell culture and tissue engineering: towards natural therapeutics, Bioeng. Trans. Med 4 (2018) 96–115.

[37]. Hajiali H, Shahgasempour S, Naimi-Jamal MR, Peirovi H, Electrospun PGA/gelatin nanofibrous scaffolds and their potential application in vascular tissue engineering, Int. J. Nanomed. 6 (2011) 2133–2141.

[38]. Kolehmainen K, Willerth SM, Preparation of 3D fibrin scaffolds for stem cell culture applications, JoVE (2012), e3641. [PubMed: 22415575]

[39]. Andersen T, Auk-Emblem P, Dornish M, 3D cell culture in alginate hydrogels, Microarrays 4 (2015) 133–161. [PubMed: 27600217]

[40]. Li J, Tao R, Wu W, Cao H, Xin J, Li J, Guo J, Jiang L, Gao C, Demetriou AA, Farkas DL, Li L, 3D PLGA scaffolds improve differentiation and function of bone marrow mesenchymal stem cell-derived hepatocytes, Stem Cell. Dev. 19 (2010) 1427–1436.

[41]. Pu F, Rhodes NP, Bayon Y, Chen R, Brans G, Benne R, Hunt JA, The use of flow perfusion culture and subcutaneous implantation with fibroblast-seeded PLLA-collagen 3D scaffolds for abdominal wall repair, Biomaterials 31 (2010) 4330–4340. [PubMed: 20219244]

[42]. Hu J, Sun X, Ma H, Xie C, Chen YE, Ma PX, Porous nanofibrous PLLA scaffolds for vascular tissue engineering, Biomaterials 31 (2010) 7971–7977. [PubMed: 20673997]

[43]. Wei G, Ma PX, Partially nanofibrous architecture of 3D tissue engineering scaffolds, Biomaterials 30 (2009) 6426–6434. [PubMed: 19699518]

[44]. Holland C, Numata K, Rnjak-Kovacina J, Seib FP, The biomedical use of silk: past, present, future, Adv. Healthc. Mater. 8 (2019) 1800465.

[45]. Chung YG, Algarrahi K, Franck D, Tu DD, Adam RM, Kaplan DL, Estrada CR Jr., Mauney JR, The use of bi-layer silk fibroin scaffolds and small intestinal submucosa matrices to support bladder tissue regeneration in a rat model of spinal cord injury, Biomaterials 35 (2014) 7452–7459. [PubMed: 24917031]

[46]. Sack B, Mauney J, Estrada C, Silk fibroin scaffolds for urologic tissue engineering, Curr. Urol. Rep 17 (2016) 1–10. [PubMed: 26686192]

[47]. Sharma K, Mujawar MA, Kaushik A, State-of-Art functional biomaterials for tissue engineering, Front. Mater 6 (2019).

[48]. Song Y, Wang H, Yue F, Lv Q, Cai B, Dong N, Wang Z, Wang L, Silk-based biomaterials for cardiac tissue engineering, Adv. Healthc. Mater 9 (2020) 2000735.

[49]. Ding H, Zhong J, Xu F, Song F, Yin M, Wu Y, Hu Q, Wang J, Establishment of 3D culture and induction of osteogenic differentiation of pre-osteoblasts using wet-collected aligned scaffolds, Mater. Sci. Eng. C Mater. Biol. Appl 71 (2017) 222–230. [PubMed: 27987702]

[50]. Loh QL, Choong C, Three-dimensional scaffolds for tissue engineering applications: role of porosity and pore size, Tissue Eng. Part B, Rev. 19 (2013) 485–502. [PubMed: 23672709]

[51]. Varga ZV, Ferdinandy P, Liaudet L, Pacher P, Drug-induced mitochondrial dysfunction and cardiotoxicity, Am. J. Physiol. Heart Circ. Physiol. 309 (2015) H1453–H1467. [PubMed: 26386112]

[52]. Kamalian L, Douglas O, Jolly CE, Snoeys J, Simic D, Monshouwer M, Williams DP, Kevin Park B, Chadwick AE, The utility of HepaRG cells for bioenergetic investigation and detection of drug-induced mitochondrial toxicity, Toxicol. Vitro 53 (2018) 136–147.

[53]. Rana P, Aleo MD, Gosink M, Will Y, Evaluation of in vitro mitochondrial toxicity assays and physicochemical properties for prediction of organ toxicity using 228 pharmaceutical drugs, Chem. Res. Toxicol. 32 (2019) 156–167. [PubMed: 30525499]

[54]. Dalakas MC, Semino-Mora C, Leon-Monzon M, Mitochondrial alterations with mitochondrial DNA depletion in the nerves of AIDS patients with peripheral neuropathy induced by 2’3’-dideoxycytidine (ddC), Lab. Invest. 81 (2001) 1537–1544. [PubMed: 11706061]

[55]. Zhang Y, McNeill E, Tian H, Soker S, Andersson K-E, Yoo JJ, Atala A, Urine derived cells are a potential source for urological tissue reconstruction, J. Urol. 180 (2008) 2226–2233. [PubMed: 18804817]

[56]. Bharadwaj S, Liu G, Shi Y, Wu R, Yang B, He T, Fan Y, Lu X, Zhou X, Liu H, Atala A, Rohozinski J, Zhang Y, Multipotential differentiation of human urine-derived stem cells: potential for therapeutic applications in urology, Stem Cell. 31 (2013) 1840–1856.

[57]. Bharadwaj S, Liu G, Shi Y, Markert C, Andersson KE, Atala A, Zhang Y, Characterization of urine-derived stem cells obtained from upper urinary tract for use in cell-based urological tissue engineering, Tissue Eng. 17 (2011) 2123–2132.

[58]. Zhang D, Wei G, Li P, Zhou X, Zhang Y, Urine-derived stem cells: a novel and versatile progenitor source for cell-based therapy and regenerative medicine, Genes Dis. 1 (2014) 8–17. [PubMed: 25411659]

[59]. Dong X, Zhang T, Liu Q, Zhu J, Zhao J, Li J, Sun B, Ding G, Hu X, Yang Z, Zhang Y, Li L, Beneficial effects of urine-derived stem cells on fibrosis and apoptosis of myocardial, glomerular and bladder cells, Mol. Cell. Endocrinol. 427 (2016) 21–32. [PubMed: 26952874]

[60]. Guo H, Deng N, Dou L, Ding H, Criswell T, Atala A, Furdui CM, Zhang Y, 3-D Human Renal Tubular Organoids Generated from Urine-Derived Stem Cells for Nephrotoxicity Screening, ACS Biomaterials Science & Engineering, 2020.

[61]. Yang Q, Chen W, Han D, Zhang C, Xie Y, Sun X, Liu G, Deng C, Intratunical injection of human urine-derived stem cells derived exosomes prevents fibrosis and improves erectile function in a rat model of Peyronie’s disease, Andrologia (2020), e13831. [PubMed: 32986908]

[62]. Zhou C, Wu X-R, Liu H-S, Liu X-H, Liu G-H, Zheng X-B, Hu T, Liang Z-X, He X-W, Wu X-J, Smith LC, Zhang Y, Lan P, Immunomodulatory effect of urine-derived stem cells on inflammatory bowel diseases via down-regulating Th1/Th17 immune responses in a PGE2-dependent manner, J. Crohn’s Colitis 14 (2019) 654–668.

[63]. Liu G, Wu R, Yang B, Shi Y, Deng C, Atala A, Mou S, Criswell T, Zhang Y, A cocktail of growth factors released from a heparin hyaluronic-acid hydrogel promotes the myogenic potential of human urine-derived stem cells in vivo, Acta Biomater. 107 (2020) 50–64. [PubMed: 32044457]

[64]. Yang Q, Chen X, Zheng T, Han D, Zhang H, Shi Y, Bian J, Sun X, Xia K, Liang X, Liu G, Zhang Y, Deng C, Transplantation of human urine-derived stem cells transfected with pigment epithelium-derived factor to protect erectile function in a rat model of cavernous nerve injury, Cell Transplant. 25 (2016) 1987–2001. [PubMed: 27075964]

[65]. Xiong G, Tao L, Ma WJ, Gong MJ, Zhao L, Shen LJ, Long CL, Zhang DY, Zhang YY, Wei GH, Urine-derived stem cells for the therapy of diabetic nephropathy mouse model, Eur. Rev. Med. Pharmacol. Sci 24 (2020) 1316–1324. [PubMed: 32096161]

[66]. Sun B, Luo X, Yang C, Liu P, Yang Y, Dong X, Yang Z, Xu J, Zhang Y, Li L, Therapeutic effects of human urine-derived stem cells in a rat model of cisplatin-induced acute kidney injury in vivo and in vitro, Stem Cell. Int 2019 (2019) 8035076.

[67]. Zhu Q, Li Q, Niu X, Zhang G, Ling X, Zhang J, Wang Y, Deng Z, Extracellular vesicles secreted by human urine-derived stem cells promote ischemia repair in a mouse model of hind-limb ischemia, Cell. Physiol. Biochem. 47 (2018) 1181–1192. [PubMed: 30041250]

[68]. Zhang Y, Tian H, Bharadwaj S, Liu Y, Hodges S, Atala A, Urine-derived stem cells for urological injection therapy, J. Urol. 181 (2009) 546.

[69]. Zhang Y, Niu X, Dong X, Wang Y, Li H, Bioglass enhanced wound healing ability of urine-derived stem cells through promoting paracrine effects between stem cells and recipient cells, J. Tissue Eng. Regen. Med. 12 (2018) e1609–e1622.

[70]. Zhang D, Chu J, Ma W, Gong M, Wei G, Zhang Y, Urine-derived stem cells for potential use in treatment of urethral sphincter dysfunction, Int. J. Stem Cell Res 1 (2015), 10.16966/ijscr.105.

[71]. Zhang C, George SK, Wu R, Thakker PU, Abolbashari M, Kim T-H, Ko IK, Zhang Y, Sun Y, Jackson J, Lee SJ, Yoo JJ, Atala A, Reno-protection of urine-derived stem cells in A chronic kidney disease rat model induced by renal ischemia and nephrotoxicity, Int. J. Biol. Sci. 16 (2020) 435–446. [PubMed: 32015680]

[72]. Yang H, Chen B, Deng J, Zhuang G, Wu S, Liu G, Deng C, Yang G, Qiu X, Wei P, Wang X, Zhang Y, Characterization of rabbit urine-derived stem cells for potential application in lower urinary tract tissue regeneration, Cell Tissue Res. 374 (2018) 303–315. [PubMed: 30066105]

[73]. Wu S, Liu G, Bharadwaj S, Hoagie S, Atala A, Zhang Y, 181 cell therapy with autologous urine-derived stem cells for vesicoureteral reflux, J. Urol. 185 (2011) e75.

[74]. Wu RP, Liu G, Shi YA, Bharadwaj S, Atala A, Zhang Y, Human urine-derived stem cells originate from parietal stem cells, J. Urol. 191 (2014) e1–e958.

[75]. Wan Q, Xiong G, Liu G, Shupe TD, Wei G, Zhang D, Liang D, Lu X, Atala A, Zhang Y, Urothelium with barrier function differentiated from human urine-derived stem cells for potential use in urinary tract reconstruction, Stem Cell Res. Ther 9 (2018) 304. [PubMed: 30409188]

[76]. Tran CT A, Yi H, Balog B, Zhang Y, Damaser M, Human urine-derived stem cells or their secretome alone facilitate functional recovery in a rat model of stress urinary incontinence, J. Urol. 195 (4S) (2016) e845.

[77]. Tran CNT A, Balog B, Zhang Y, Damaser M, Paracrine effects of human urine-derived stem cells in treatment of female stress urinary incontinence in a rodent model, Tissue Eng. 21 (2015) S–S385.

[78]. Qin H, Zhu C, An Z, Jiang Y, Zhao Y, Wang J, Liu X, Hui B, Zhang X, Wang Y, Silver nanoparticles promote osteogenic differentiation of human urine-derived stem cells at noncytotoxic concentrations, Int. J. Nanomed 9 (2014) 2469–2478.

[79]. Qin D, Long T, Deng J, Zhang Y, Urine-derived stem cells for potential use in bladder repair, Stem Cell Res. Ther 5 (2014) 69. [PubMed: 25157812]

[80]. Ouyang B, Sun X, Han D, Chen S, Yao B, Gao Y, Bian J, Huang Y, Zhang Y, Wan Z, Yang B, Xiao H, Songyang Z, Liu G, Zhang Y, Deng C, Human urine-derived stem cells alone or genetically-modified with FGF2 Improve type 2 diabetic erectile dysfunction in a rat model, PLoS One 9 (2014), e92825. [PubMed: 24663037]

[81]. Long TJ, Y.D., Shi H, Zhong LR, Zhang DY, Li W, Zhang Y, Chen D, Jiao Y, Diz D, Zhang Y, Human urine-derived stem cells lessen inflammation and fibrosis within kidney tissue in a rodent model of aging-related renal insufficiency, J. Urol. 197 (2017) e293.

[82]. Liu G, Pareta RA, Wu R, Shi Y, Zhou X, Liu H, Deng C, Sun X, Atala A, Opara EC, Zhang Y, Skeletal myogenic differentiation of urine-derived stem cells and angiogenesis using microbeads loaded with growth factors, Biomaterials 34 (2013) 1311–1326. [PubMed: 23137393]

[83]. Ling X, Zhang G, Xia Y, Zhu Q, Zhang J, Li Q, Niu X, Hu G, Yang Y, Wang Y, Deng Z, Exosomes from human urine-derived stem cells enhanced neurogenesis via miR-26a/HDAC6 axis after ischaemic stroke, J. Cell Mol. Med. 24 (2020) 640–654. [PubMed: 31667951]

[84]. Li J, Luo H, Dong X, Liu Q, Wu C, Zhang T, Hu X, Zhang Y, Song B, Li L, Therapeutic effect of urine-derived stem cells for protamine/lipopolysaccharide-induced interstitial cystitis in a rat model, Stem Cell Res. Ther 8 (2017) 107. [PubMed: 28482861]

[85]. Lang R, Liu G, Shi Y, Bharadwaj S, Leng X, Zhou X, Liu H, Atala A, Zhang Y, Self-renewal and differentiation capacity of urine-derived stem cells after urine preservation for 24 hours, PLoS One 8 (2013), e53980. [PubMed: 23349776]

[86]. Guan J, Zhang J, Guo S, Zhu H, Zhu Z, Li H, Wang Y, Zhang C, Chang J, Human urine-derived stem cells can be induced into osteogenic lineage by silicate bioceramics via activation of the Wnt/beta-catenin signaling pathway, Biomaterials 55 (2015) 1–11. [PubMed: 25934447]

[87]. Fu Y, Guan J, Guo S, Guo F, Niu X, Liu Q, Zhang C, Nie H, Wang Y, Human urine-derived stem cells in combination with polycaprolactone/gelatin nanofibrous membranes enhance wound healing by promoting angiogenesis, J. Transl. Med 12 (2014) 274. [PubMed: 25274078]

[88]. Liu G, Wu R, Yang B, Deng C, Lu X, Walker SJ, Ma PX, Mou S, Atala A, Zhang Y, Human urine-derived stem cell differentiation to endothelial cells with barrier function and nitric oxide production, Stem Cells Trans. Med 7 (2018) 686–698.

[89]. Noel P, Muñoz R, Rogers GW, Neilson A, Von Hoff DD, Han H, Preparation and metabolic assay of 3-dimensional spheroid Co-cultures of pancreatic cancer cells and fibroblasts, JoVE : JoVE (2017) 56081.

[90]. Russell S, Wojtkowiak J, Neilson A, Gillies RJ, Metabolic Profiling of healthy and cancerous tissues in 2D and 3D, Sci. Rep. 7 (2017) 15285. [PubMed: 29127321]

[91]. van der Stel W, Carta G, Eakins J, Darici S, Delp J, Forsby A, Bennekou SH, Gardner I, Leist M, Danen EHJ, Walker P, van de Water B, Jennings P, Multiparametric assessment of mitochondrial respiratory inhibition in HepG2 and RPTEC/TERT1 cells using a panel of mitochondrial targeting agrochemicals, Arch. Toxicol. 94 (2020) 2707–2729. [PubMed: 32607615]

[92]. Kang C, Xu Q, Martin TD, Li MZ, Demaria M, Aron L, Lu T, Yankner BA, Campisi J, Elledge SJ, The DNA damage response induces inflammation and senescence by inhibiting autophagy of GATA4, Science 349 (2015) aaa5612. [PubMed: 26404840]

[93]. Rooney JP, Ryde IT, Sanders LH, Howlett EH, Colton MD, Germ KE, Mayer GD, Greenamyre JT, Meyer JN, PCR based determination of mitochondrial DNA copy number in multiple species, Methods Mol. Biol. 1241 (2015) 23–38. [PubMed: 25308485]

[94]. Ploumi C, Daskalaki I, Tavernarakis N, Mitochondrial biogenesis and clearance: a balancing act, FEBS J. 284 (2017) 183–195. [PubMed: 27462821]

[95]. Weinbaum S, Duan Y, Satlin LM, Wang T, Weinstein AM, Mechanotransduction in the renal tubule, Am. J. Physiol. Ren. Physiol. 299 (2010) F1220–F1236.

[96]. Brown AN, Drusano GL, Adams JR, Rodriquez JL, Jambunathan K, Baluya DL, Brown DL, Kwara A, Mirsalis JC, Hafner R, Louie A, Preclinical evaluations to identify optimal linezolid regimens for tuberculosis therapy, mBio 6 (2015) e01741–e01815. [PubMed: 26530386]

[97]. Jolly CE, Douglas O, Kamalian L, Jenkins RE, Beckett AJ, Penman SL, Williams DP, Monshouwer M, Simic D, Snoeys J, Park BK, Chadwick AE, The utility of a differentiated preclinical liver model, HepaRG cells, in investigating delayed toxicity via inhibition of mitochondrial-replication induced by fialuridine, Toxicol. Appl. Pharmacol. 403 (2020) 115163. [PubMed: 32730777]

[98]. Madorran E, Stožer A, Bevc S, Maver U, In vitro toxicity model: upgrades to bridge the gap between preclinical and clinical research, Bosn. J. Basic Med. Sci. 20 (2020) 157–168. [PubMed: 31621554]

[99]. Yu P, Duan Z, Liu S, Pachon I, Ma J, Hemstreet GP, Zhang Y, Drug-induced nephrotoxicity assessment in 3D cellular models, Micromachines 13 (2021).

[100]. Will Y, Shields JE, Wallace KB, Drug-induced mitochondrial toxicity in the geriatric population: challenges and future directions, Biology 8 (2019) 32.

[101]. Schank M, Zhao J, Moorman JP, Yao ZQ, The impact of HIV- and ART-induced mitochondrial dysfunction in cellular senescence and aging, Cells (2021) 10.

[102]. Chen CH, Vazquez-Padua M, Cheng YC, Effect of anti-human immunodeficiency virus nucleoside analogs on mitochondrial DNA and its implication for delayed toxicity, Mol. Pharmacol. 39 (1991) 625–628. [PubMed: 1851960]

[103]. Yamanaka H, Gatanaga H, Kosalaraksa P, Matsuoka-Aizawa S, Takahashi T, Kimura S, Oka S, Novel mutation of human DNA polymerase γ associated with mitochondrial toxicity induced by anti-HIV treatment, J. Infect. Dis. 195 (2007) 1419–1425. [PubMed: 17436221]

[104]. Birkus G, Hitchcock MJ, Cihlar T, Assessment of mitochondrial toxicity in human cells treated with tenofovir: comparison with other nucleoside reverse transcriptase inhibitors, Antimicrob. Agents Chemother. 46 (2002) 716–723. [PubMed: 11850253]

[105]. Ramaiahgari SC, Ferguson SS, in: Vinken M (Ed.), Organotypic 3D HepaRG Liver Model for Assessment of Drug-Induced Cholestasis. Experimental Cholestasis Research, Springer New York, New York, NY, 2019, pp. 313–323.

[106]. Dalakas MC, Semino-Mora C, Leon-Monzon M, Mitochondrial alterations with mitochondrial DNA depletion in the nerves of AIDS patients with peripheral neuropathy induced by 2'3'-dideoxycytidine (ddC), Lab. Invest. 81 (2001) 1537–1544. [PubMed: 11706061]

[107]. Ding H, Jambunathan K, Jiang G, Margolis DM, Leng XI, Ihnat M, Ma JX, Marsalis J, Zhang Y, 3D organoids of human primary urine-derived stem cells in the assessment of mitochondrial toxicity induced by antiretroviral therapy, Pharmaceutics 14 (2022) 1042. [PubMed: 35631624]

[108]. Cihlar T, Birkus G, Greenwalt DE, Hitchcock MJM, Tenofovir exhibits low cytotoxicity in various human cell types: comparison with other nucleoside reverse transcriptase inhibitors, Antivir. Res 54 (2002) 37–45. [PubMed: 11888656]

[109]. Jensen C, Teng Y, Is it time to start transitioning from 2D to 3D cell culture? Front. Mol. Biosci 7 (2020).

[110]. Lin KH, Xie A, Rutter JC, Ahn YR, Lloyd-Cowden JM, Nichols AG, Soderquist RS, Koves TR, Muoio DM, MacIver NJ, Lamba JK, Pardee TS, McCall CM, Rizzieri DA, Wood KC, Systematic dissection of the metabolic-apoptotic interface in AML reveals heme biosynthesis to Be a regulator of drug sensitivity, Cell Metabol. 29 (2019) 1217–12131 e7.

[111]. Campioni G, Pasquale V, Busti S, Ducci G, Sacco E, Vanoni M, An optimized workflow for the analysis of metabolic fluxes in cancer spheroids using Seahorse technology, Cells (2022) 11.

Statement of significance

Despite being commonly used to produce scaffolds for tissue regeneration, the silk fiber matrix (SFM) with human primary cells developed in this study is the first use in a long-term culture (>6 weeks) predicting drug-induced chronic mitochondrial toxicity. Therefore, it has great promise for both new drug assessment and personalized toxicology. Key innovations of this study include human primary urinary stem cells seeded 3D SFM (3D USC-SFM):

- offers stable cell growth, mitochondrial copy numbers in 3D culture for 6 weeks, which is suitable for determining drug-induced chronic MtT;
- provides a cost-effective and sensitive assay to test MtT by increasing the yield of USC in 3D silk fiber network 125-fold, compared to spheroids;
- performs multiple assays from one large cell sample that makes the results more reliable and accurate with less variability;
- could be used in prediction of chronic MtT using patient's own cells for personalized toxicology;
- could be used in testing drug-induced nephrotoxicity as USC are renal progenitor cells.

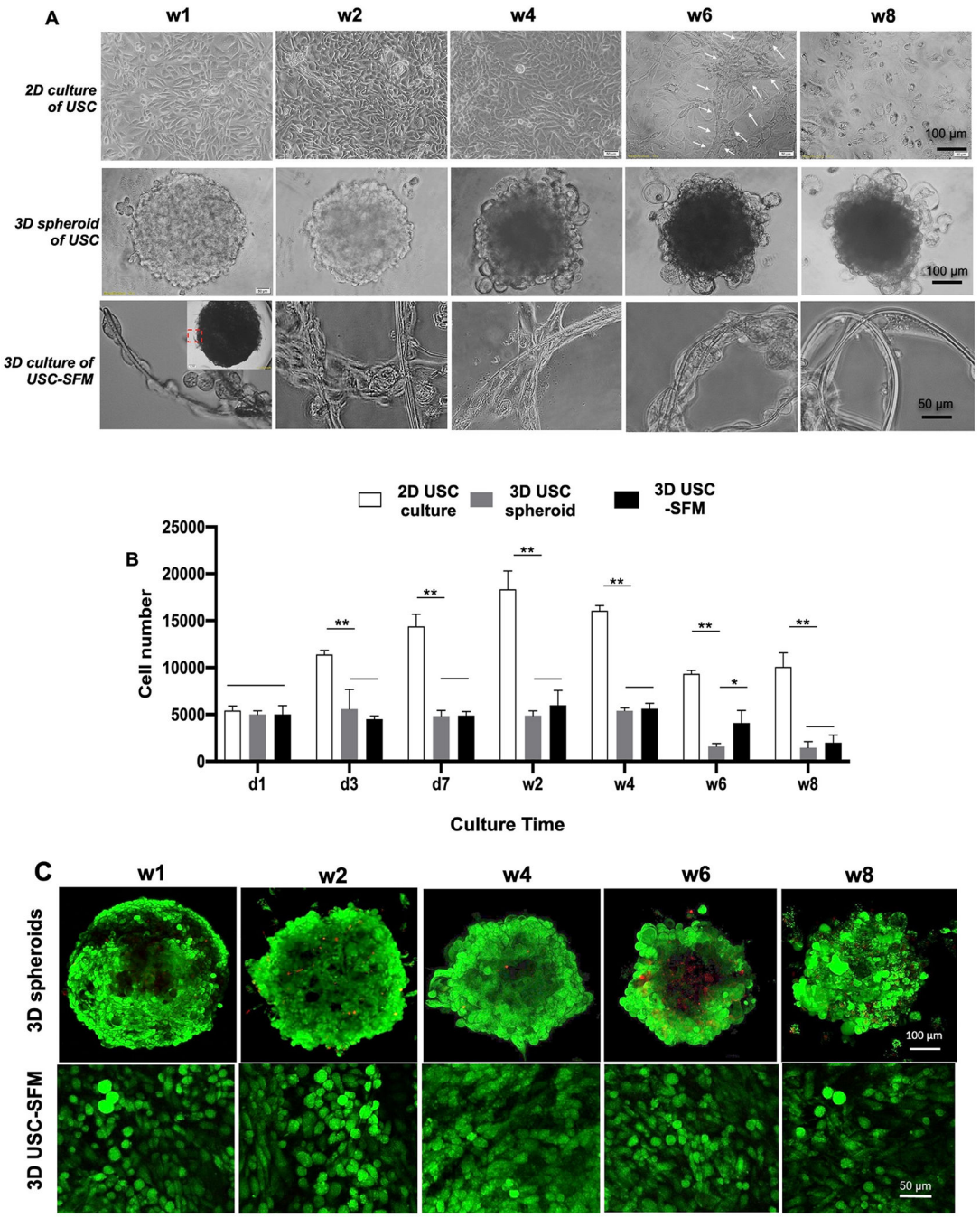

Fig. 1.

Morphology and viability of 3D USC-SFM during long-term culture. A) Morphology of USC in three culture conditions with time. USC at p4 grew on silk fibers of s-SFM, 3D spheroids remained stable size in ultra-low attachment 96-well plate. USC reached over-confluent status with time in 2D culture, when USC were initially seeded at 4 × 10 [3] at culture conditions (3D sSFM at Ø4mm × 0.2 mm, spheroid and 2D culture in 96-well) plate at different time points, under phase contrast microscope. B) Cell proliferation of USC in 3D SFM. USC culture (initial seeding cell number 4 × 10 [3]) at day 1, 3, 7 and week 2,

4, 6, and 8, assessed by CCK-8 test. *$p < 0.05$. C) Cell viability of USC in 3D cultures at different time points. In 3D SFM, most USC (95%) survived up to 8 weeks although there was about 20% of cells density decrease at 8 weeks, compared to cultures at 6 weeks. In 3D spheroids, most cells appeared healthy at week 4 but the number of died cells increased at week 6. The size of USC spheroids presented slightly larger in the first week, remained stable at week 2 and 4, and decreased with time starting at week 6. It formed necrosis at the center of spheres at week 8 (assessed by live/dead kit).

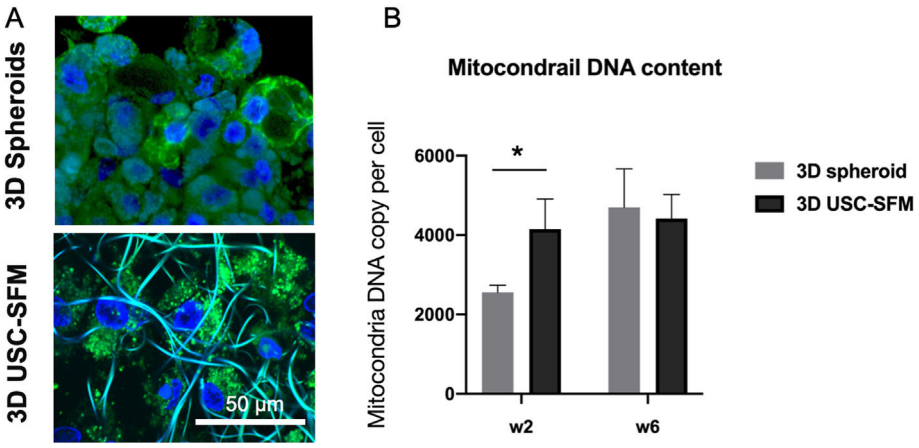

Fig. 2.

Mitochondrial mass and DNA content (mtDNA content) in 3D cultures. A) No statistical difference in mtDNA content/cell between 3D spheroids and 3D USC-SFM at weeks 6 ($p > 0.05$). The levels of mtDNA content in 3D of USC-SFM are similar between week 2 and 6, assessed by q-PCR. (4×10 [3] cells/well in ULA 96-well plate, n = 3/sample, $^*p < 0.05$). B) Mito-Tracker Green staining of mitochondria in 3D spheroids and 3D USC-SFM at 6 weeks.

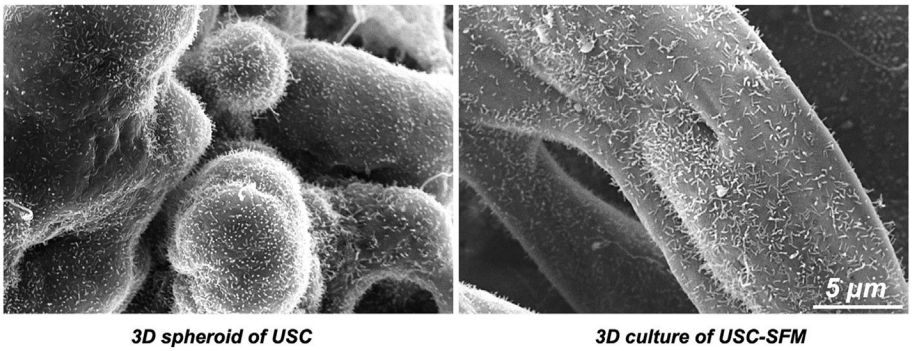

Fig. 3.

Ultrastructure of USC in 3D cultures. Rich microvilli on the apical side of the USC grew along the silk fibers and intracellular spaces are found among the cell-silk fiber networks, compared to USC with similar microvilli on surface of 3D spheroids at 4 weeks after culture, as assessed by scanning electron microscopy.

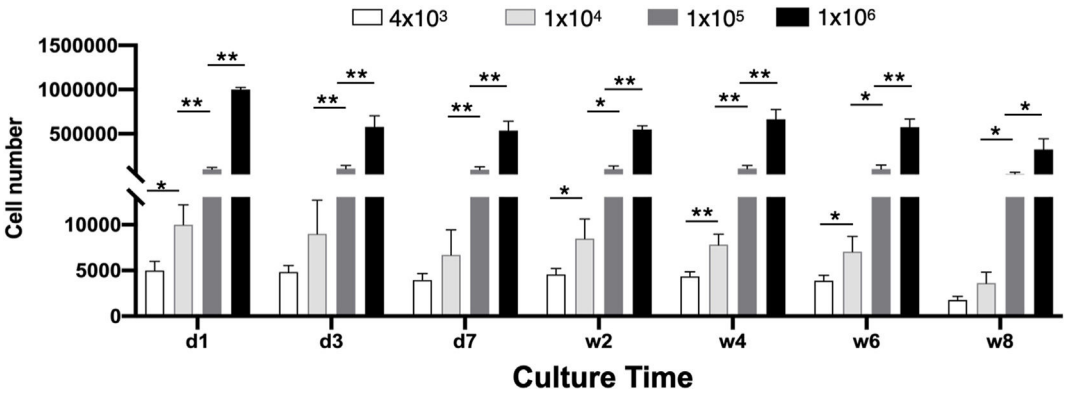

Fig. 4.

Optimization of cell concentrations in 3D USC-SFM during long-term culture. Number of USC at different cell concentrations at p4 seeded on SFM (Ø at 4 mm × 0.2mm/well in 96-well plates, n = 3) for 8 weeks was assessed by CCK-8, indicating that the maximal number of cells that can be loaded in SFM in a 96-well plate is 1 × 10 [5] cells/1.3 mm^3 SFM/well. When more cells (e.g., 10^6 cells/25.2 mm^3 SFM/well) were loaded into large size SFM retained only 1 × 10 [5] cells up to 8 weeks.

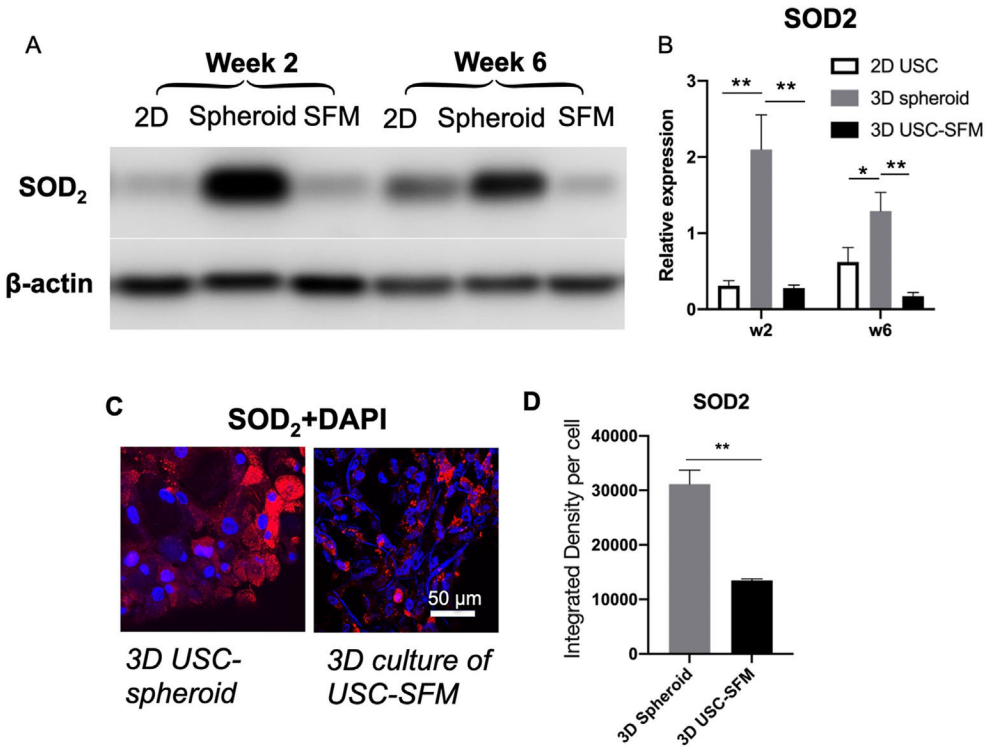

Fig. 5.

Significant increases in superoxide dismutase 2 (SOD2) expression in spheroids, but not in 3D USC-SFM. A) Protein levels of mitochondrial SOD2 significantly increased in 3D USC spheroids, compared to that in 3D USC-SFM and 2D culture at weeks 2 and 6. This was assessed by Western blot. B). The semi-quantification analysis for SOD2 in cell lysates shown for (A) The intensity of the bands in each cell culture model was calculated relative to β-Actin housekeeping protein. Data (n = 3 samples) were expressed as means ± SD. C) Expression level of SOD2 in mitochondria significantly increased in 3D organoids of USC at week 4, compared to that of USC-SFM (n = 5, $p < 0.05$). The initial seeding cell number was 4 × 10 [3] cells in SFM at Ø 4 mm × 0.2 mm) in a 96-well-plate, assessed by double immune-fluorescent staining (SOD2/DAPI). D) semi-quantification analysis for (C).

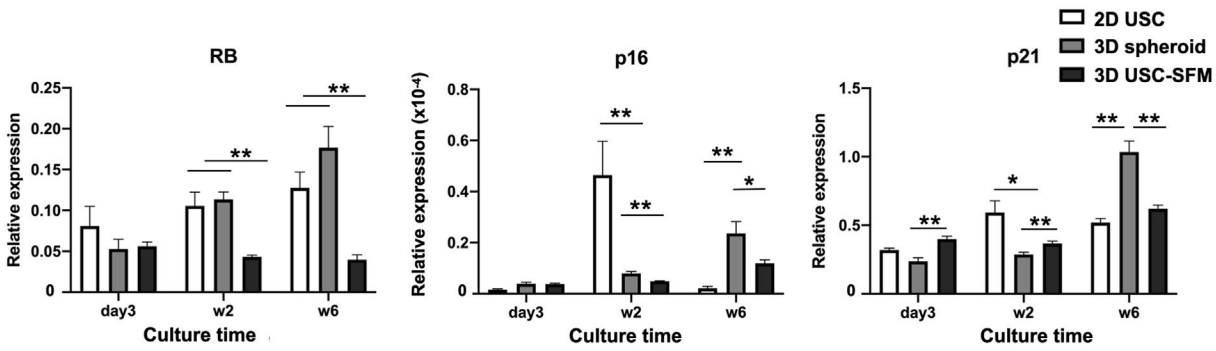

Fig. 6.

Senescence-related gene expression of USC in 3D cultures. Quantitative PCR analysis showed the mRNA levels (RB and P16, p21) of USC in 2D culture, 3D spheroids and 3D SFM from three individuals at day 3, week 2 and week 6, respectively. The results were expressed as mean ± SD of three independent experiments. Asterisks indicate significant differences (*$p < 0.05$, **$p < 0.01$). Senescence-related genes in 3D USC-SFM were significantly lower compared to those in 3D USC spheroids at week 6.

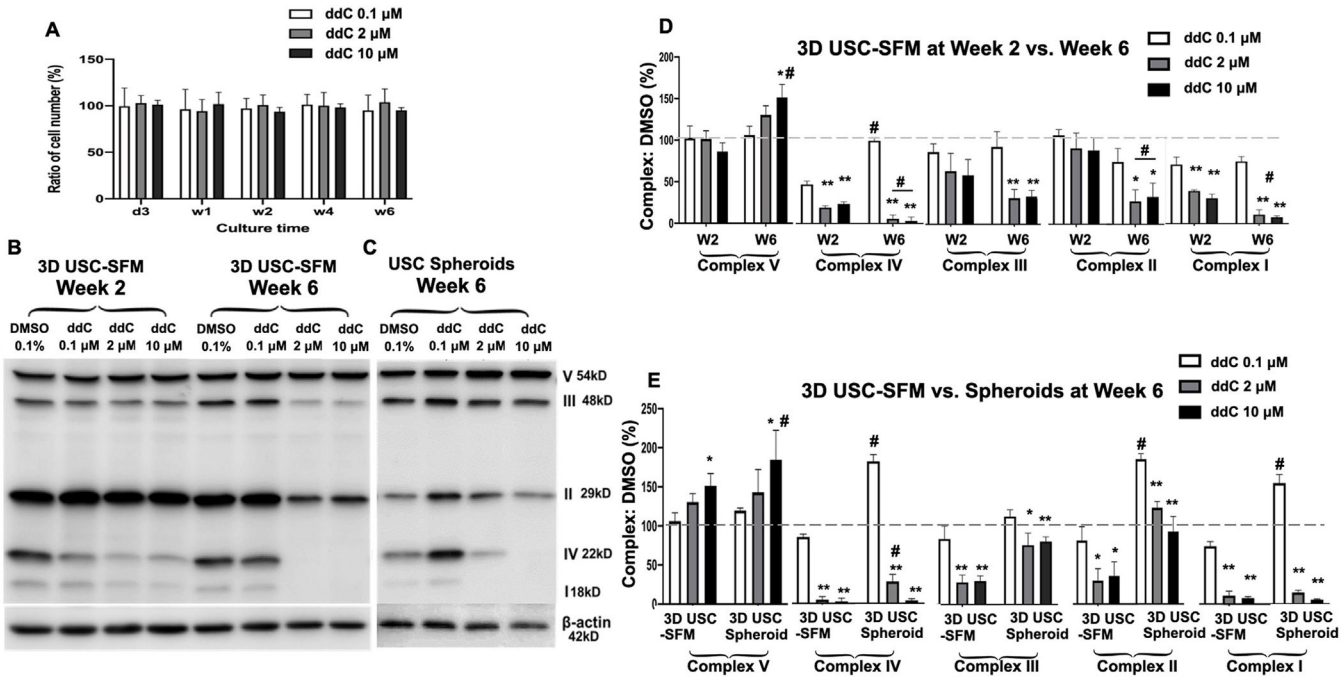

Fig. 7.

Dysfunctional electron transport chain (ETC) complexes I–V in 3D USC cultures 6 weeks after ddC treatment. A) Cell viability of 3D culture of USC-SFM treated with ddC over time. USC at p4 seeded on 3D SFM at weeks 2 and 6, assessed by CCK-8. B) Western blot protein expression of ETC complex I (NDUFB8), complex II (SDHB), III (UQCRC2), IV (COXII) and V (V-ATP5A) in 3D culture of USC-SFM (n = 3 samples/treatment) treated with ddC at different doses at weeks 2 and 6). C) Protein expression levels of ETC complex I-IV between 3D USC-SFM and spheroids treated with ddC at the same time point (week 6) were compared to those in DMSO control. D) The semi-quantification analysis of the bands in B to compare the protein levels of complexes I–V in 3D USC-SFM 2 and 6 weeks after being treated with ddC. Complex I-IV significantly decreased in USC-SFM treated with ddC at 2 and 20 μM compared to low dose (0.1 μM) ddC and DMSO control at week 6. In addition, levels of complex IV, II and I were significantly lower at week 6 (#$p < 0.05$), compared to those at week 2. E) The semi-quantification analysis for C compares the protein levels of complex I–V in 3D USC-SFM and spheroids at week 6. Expression levels of complex I-IV significantly decrease in USC treated with ddC (2 and 20 μM) in both 3D USC-SFM and spheroid models, compared to those treated with ddC at 0.1 μM and DMSO. In addition, levels of complex II and IV in 3D USC-SFM were significantly lower than those in 3D spheroids. USC at 5 × 10 [5] cells/SFM Ø at 1 mm/well in ULA 12-well (n = 3) for 6 weeks after treated with ddC (0.1, 2, 10 μM). All the data from complex I–V bands treated USC were normalized to β-actin as a loading control. The intensity of the bands in each cell culture model was calculated relative to this value. Data (n = 3 samples) are expressed as means ± SD. Student's T-test was used. *$p < 0.05$; **$p < 0.01$; #$p < 0.05$.

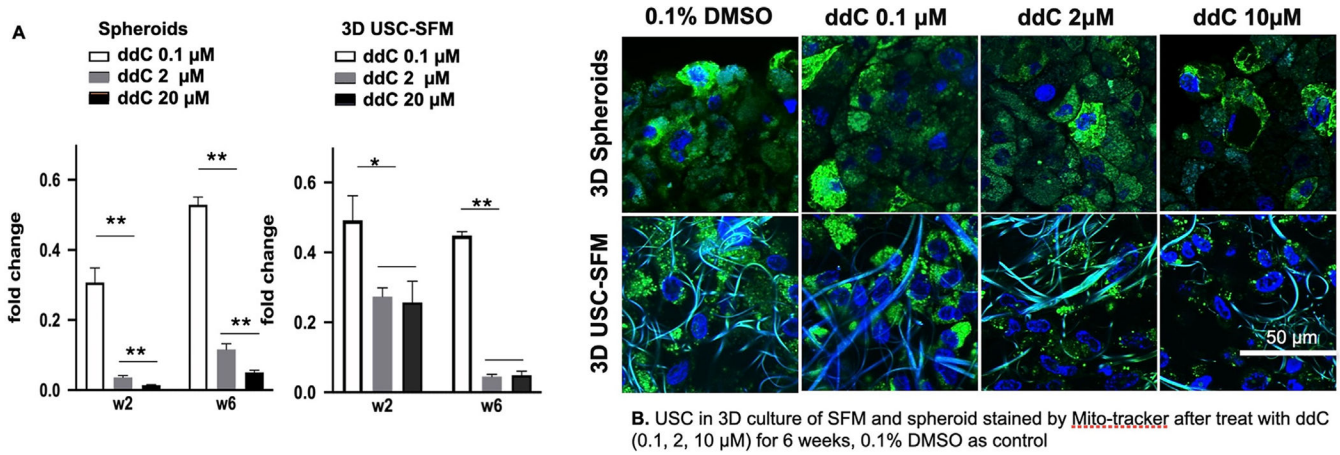

Fig. 8.

Mitochondrial DNA content and mass significantly decrease with increased ddC doses in 3D culture of USC over time. **A**) Changes in mtDNA content of USC treated with ddC. Levels of mtDNA content significantly decreased in 3D spheroid of USC and 3D USC-SFM 2 and 6 weeks after being treated with ddC at three different doses (0.2, 2, or 20 μM), compared to cells treated with DMSO standardized as 100%. ddC at 2 or 20 μM significantly inhibited mtDNA content compared to those treated 0.1 μM ddC. Decreased mtDNA content displayed a dose-dependent manner in 3D spheroids of USC; decreased mtDNA content showed in a time-depended manner in 3D USC-SFM, which was assessed by q-PCR. Fold change of relative mtDNA content was compared to control (0.1% DMSO) n = 3 samples) after the values were normalized to nuclear DNA. **B**) Mitochondrial mass of USC decreased with increasing ddC doses in both 3D USC-SFM and spheroids. This was determined by Mito-tracker staining after treatment with ddC (0.1, 2, 10 μM) for 6 weeks where 0.1% DMSO served as control. USC at 4 × 10 [3] cells/well were cultured in ULA 96-well plates. Significance was set at $p < 0.05$ and all data were represented as mean ± SD. *$p < 0.05$ and **$p < 0.01$.

Table 1

3D culture systems of USC were used in this study.

	3D USC-SFM		3D USC spheroids
	Large size SFM (l-SFM)	**Small size SFM (s-SFM)**	
Cell no./well	5 × 10 [5]/Ø8mm/well, 1 mm thickness in ULA 12-well Plate	4 × 10 [3]/Ø4 mm/well, 0.2 mmthickness in ULA 96-well plate	4 × 10 [3]/well in ULA 96-well plate
Cell culture time periods	6 weeks	6 weeks	4 weeks
Suitable for toxicological parameters	• Complex I–V and SOD_2 assessed by Western-blot and immunostaining • mt-DNA content, cell Senescence-related genes by q-PCR	• Morphology assessed by phrase contrast, • Cell growth curve or cell viability by cck8 and live/dead kits • Ultrastructure by SEM	• Active mitochondria assessed by Mito-Tracker green with immunostaining • Cellular respiration and lactate release assessed by seahorse technology [89–91]

Abbreviations: ULA, ultralow attachment; cck8, Cell Counting Kit 8; mt-DNA, mitochondrial deoxyribonucleic acid; q-PCR, real-time polymerase chain reaction; FCM-flow cytometry; Immumo-staining, immune-fluorescent staining; SEM, scan electron microscope; MtT, mitochondrial toxicity.

Table 2

Primers used in q-PCR analysis.

mtDNA Content		
Hu Mt	Forward primer	CACCCAAGAACAGGGTTTGT
	Reverse primer	TGGCCATGGGTATGTTGTTA
Hu Nu	Forward primer	TGCTGTCTCCATGTTTGATGTATCT
	Reverse primer	TCTCTGCTCCCCACCTCTAAGT
Cell senescence genes		
P16	Forward primer	ATGGAGCCTTCGGCTGACT
	Reverse primer	GTAACTATTCGGTGCGTTGGG
p21	Forward primer	TGTCCGTCAGAACCCATGC
	Reverse primer	AAAGTCGAAGTTCCATCGCTC
RB	Forward primer	TTGGATCACAGCGATACAAACTT
	Reverse primer	AGCGCACGCCAATAAAGACAT
Reference genes		
POLR2A	Forward primer	GCGGAATGGAAGCACGTTAAT
	Reverse primer	CCCAGCACAAAACACTCCTC
PGK1	Forward primer	GAACAAGGTTAAAGCCGAGCC
	Reverse primer	GTGGCAGATTGACTCCTACCA
GAPDH	Forward primer	CATGTTCGTCATGGGGTGAACCA
	Reverse primer	AGTGATGGCATGGACTGTGGTCAT

All Primers were purchased from Integrated DNA Technologies.

Table 3

Reagents used for Western-blot analysis.

	Vendor	dilution	Catalog #
Total OXPHOS (I–V) [41]	Abcam, USA	1:1000	ab110411
SOD_2	Cell Signaling Technology, USA	1:1000	13,141
β-Actin	Santa Cruz biotechnology	1:1000	sc-47778
Goat anti-Rabbit	Biotium	1:2000	20,405
Goat anti-Mouse	Biotium	1:2000	20,404

Table 4

Innovative characteristics of 3D USC-SFM for potential use in chronic MtT assessment.

Five Key innovations
- Establish long-term 3D cultures of human primary stem cells from healthy donors or patients
- Supports a longer-term (6-weeks) culture of USC via inhibition of senescence genes
- Provide a cost-effective assay to test chronic MtT by increasing the yield of USC in 3D SFM 125-fold, compared to USC spheroids
- Perform multiple assays from one large cell sample that makes the results more reliable and accurate with less variability
- Test ART-induced nephrotoxicity as USC are renal progenitor cells
Novel traits of USC assays
- Obtained noninvasively in low-cost setting
- Don't require enzyme for tissue dissociation, preserving cell viability
- USC expressing telomerase activity display robust regeneration potential, large-scale cell expansion, with less inter-donor variability
- Contain rich mitochondria for assessing MtT
- Hypoxia resistance leads to suitable growth in 3D culture

Table 5

In Vitro 3D culture of USC-SFM for MtT assessment.

-Control Drugs	-NRTIs known to induce significant MtT: ddC » d4T > ddI > AZT; -NRTIs known to induce minimal MtT: FTC and TAF;
-New drugs	INSTI drugs with unknown MtT induction potential: DTG, BIC, RAL, EVG Drugs with controversial MtT: PI- darunavir; NRTTI- islatravir.
-Positive control	Drugs known to induce MtT: Rotenone, Tamoxifen, and Menadione
-Negative control	Drugs that do not induce MtT nor nephrotoxicity: DMSO (0.1%)

Notes: NRTIs (known MtT: zalcitabine [ddC]» stavudine [D4T]> didanosine [ddI]> zidovudine [AZT]; minimal MtT: emtricitabine [FTC] and tenofovir alafenamide [TAF]. Clinical studies of TAF have demonstrated a much more favorable renal side-effect profiles; b) four new ART with unknown MtT (i.e., INSTIs: DTG, bictegravir [BIC], RAL, and EVG]; a NRTTI-islatravir; and a PI- darunavir), compared to positive controls (rotenone [RTNN], tamoxifen, menadione) and negative controls (0.1% DMSO).